Aerosol Science and Technology

ISSN: 0278-6826 (Print) 1521-7388 (Online) Journal homepage: https://www.tandfonline.com/loi/uast20

New Methodology for Quantifying Polycyclic Aromatic Hydrocarbons (PAHs) Using High-Resolution Aerosol Mass Spectrometry

Courtney L. Herring, Celia L. Faiola, Paola Massoli, Donna Sueper, Matthew H. Erickson, Jacob D. McDonald, Christopher D. Simpson, Michael G. Yost, B. Thomas Jobson & Timothy M. VanReken

To cite this article: Courtney L. Herring, Celia L. Faiola, Paola Massoli, Donna Sueper, Matthew H. Erickson, Jacob D. McDonald, Christopher D. Simpson, Michael G. Yost, B. Thomas Jobson & Timothy M. VanReken (2015) New Methodology for Quantifying Polycyclic Aromatic Hydrocarbons (PAHs) Using High-Resolution Aerosol Mass Spectrometry, Aerosol Science and Technology, 49:11, 1131-1148, DOI: 10.1080/02786826.2015.1101050

To link to this article: https://doi.org/10.1080/02786826.2015.1101050

Aerosol Science and Technology, 49:1131–1148, 2015

ISSN: 0278-6826 print / 1521-7388 online
DOI: 10.1080/02786826.2015.1101050

New Methodology for Quantifying Polycyclic Aromatic Hydrocarbons (PAHs) Using High-Resolution Aerosol Mass Spectrometry

Courtney L. Herring,[1] Celia L. Faiola,[2,*] Paola Massoli,[3] Donna Sueper,[3,4] Matthew H. Erickson,[2,] Jacob D. McDonald,[5] Christopher D. Simpson,[6] Michael G. Yost,[6] B. Thomas Jobson,[2] and Timothy M. VanReken[2]**

[1]*Gene and Linda Voiland School of Chemical Engineering and Bioengineering, Washington State University, Pullman, Washington, USA*
[2]*Laboratory for Atmospheric Research, Department of Civil and Environmental Engineering, Washington State University, Pullman, Washington, USA*
[3]*Aerodyne Research Inc., Billerica, Massachusetts, USA*
[4]*Cooperative Institute for Environmental Sciences, University of Colorado at Boulder, Boulder, Colorado, USA*
[5]*Lovelace Respiratory Research Institute, Albuquerque, New Mexico, USA*
[6]*Department of Environmental and Occupational Health Sciences, University of Washington, Seattle, Washington, USA*

This article presents a new methodology to potentially quantify polycyclic aromatic hydrocarbon (PAH) isomers using high-resolution time of flight aerosol mass spectrometer (HR-AMS). The fragmentation of PAHs within the HR-AMS is such that significant signal remains at the molecular ion. After quantifying the molecular ion signal and taking into account potential interferences, the amount of the parent PAH in the aerosol may be inferred once its fragmentation pattern is also known. The potential of this approach was evaluated using mixed gasoline and diesel engine exhaust sampled under varying conditions. This dataset led to the identification and quantification within the aerosol mass spectra of the molecular ions associated with 53 PAH isomers, including both unsubstituted and functionalized species. An evaluation of anticipated interferences shows that interferences from larger molecular weight PAHs (i.e., PAH/PAH interferences) could be constrained based on the fragmentation behavior of PAHs from existing HR-AMS laboratory spectra. Other signal interferences for this data set are typically less than 5% of the total signal or, for ^{13}C isotopic interferents, are well constrained by measurements of the dominant isotope. The experimental data reveal that the fractional PAH molecular ion signal remained stable despite dramatic temporal variability of the total particulate organic signal. The fractional contributions of the molecular ions for grouped PAH species and even individual compounds were remarkably consistent across experiments. The distribution of PAHs showed no apparent dependence on engine load or exhaust type. Full application of this approach will require a greater number of standard HR-AMS spectra for PAHs, so that the relationship between compounds and their molecular ions may be understood more precisely.

Received 2 April 2015; accepted 8 September 2015
*Current affiliation: Department of Applied Physics, University of Eastern Finland, Kuopio, Finland
**Current affiliation: Houston Advanced Research Center, Houston, Texas, USA
*Address correspondence to Timothy M. VanReken, Civil and Environmental Engineering, Washington State University, 405 Spokane St., Pullman, WA 99164, USA. Email: vanreken@wsu.edu

Color versions of one or more of the figures in the article can be found online at www.tandfonline.com/uast.

1. INTRODUCTION

Emissions from diesel and gasoline vehicle engines are a major source of urban air pollution, releasing a complex combination of gaseous pollutants and particulate matter (PM) to the atmosphere. The health implications of vehicle exhaust are directly tied to the chemical composition and particle size of these PM emissions (Pope et al. 2002; Adonis et al. 2003). Vehicle emissions have been chemically characterized under in-use conditions via chassis dynamometer tests (Wang et al. 2000; Nelson et al. 2008), diesel generators (Rajput and Lakhani 2009), tunnel measurements (Fraser et al. 1998; Gross et al. 2000; He et al. 2006), mobile laboratories (Canagaratna et al. 2004; Shah et al. 2004; Massoli et al. 2012), and standardized lab fuel studies (Bayona et al. 1988). One class of exhaust compounds that has been tied to adverse health

effects is the polycyclic aromatic hydrocarbons (PAHs). Many PAHs have proven carcinogenic and/or mutagenic properties (Internal Agency for Research 1989; US EPA 1992; Ravindra et al. 2008), and because of this risk they are listed among the Hazardous Air Pollutants regulated under the 1990 amendments to the United States Clean Air Act (CAAA 1990). PAHs can be present in some fuels or oils, or may form during the incomplete combustion of organic material; engine emissions are an important source, along with biomass burning, coal combustion, and cigarette and wood smoke (Polidori et al. 2008; Ravindra et al. 2008). In metropolitan areas, motor vehicles can account for as much as 90% of particle-bound PAH mass (Harrison et al. 1996; Bostrom et al. 2002).

An underlying problem in regulating PAH emissions is that the concentration and chemical speciation of vehicle exhaust PM depend on several factors linked to engine operation. These include driving conditions, driving style, ambient temperature, humidity, pressure, vehicle age, fuel type, and lubrication oil type. Trends in PAH levels in fuel and engine exhaust have been previously reported. Diesel fuel and exhaust contain higher PAH concentrations than gasoline fuel or exhaust (Mi et al. 2001; Alkurdi et al. 2013). Beyond the effects of the fuel, prior work has also suggested that PAH content in exhaust may be affected by engine load (Huang et al. 2013), cold starts (Zielinska et al. 2004; Sodeman et al. 2005), and engine oil age (Zielinska et al. 2004; Fujita et al. 2007).

In addition to the unsubstituted PAHs (UnSubPAHs), functionalized PAHs can also have significant adverse health impacts. These functionalized PAHs are either present in the fuel or lubrication oil, form during combustion, or arise from the atmospheric aging of UnSubPAHs (Atkinson and Arey 1994; Sasaki et al. 1997). Of most interest are nitrogen-substituted derivatives (NPAHs), oxygenated PAHs (OPAHs), methylated PAHs (MPAHs), and amino PAHs (APAHs). NPAHs form during the combustion cycle as a result of reactions with either HNO_3 or NO_x and have been described previously (Sienra and Rosazza 2006; Zielinska and Samy 2006; Delhomme et al. 2007; Hattori et al. 2007). OPAHs may include carboxylate, hydroxy, dihydroxy, aldehyde, carboxaldehyde, ketone, and acetoxy functional groups and can be divided into two subgroups; carboxylated PAHs that contain one or more carbonyl oxygen(s) attached to the aromatic ring (ketones and quinones) and hydroxylated PAHs containing one or more hydroxyl groups. The formation, occurrence, and chemical analysis of particle-phase OPAHs are reported by Sienra (2006). OPAHs can be formed by incomplete combustion of engine exhaust (Rappaport et al. 1980; Schuetzle et al. 1981; Choudhury 1982; Ramdahl 1983; Strandell et al. 1994). While MPAHs are often present in diesel fuel and may at times be emitted in the exhaust (Poster et al. 2003) the oxidation of these MPAHs can also lead to the formation of OPAHs (Ringuet et al. 2012). APAHs are usually the result of chemical reduction of NPAHs under low O_2 environments (Liu et al. 2007).

NPAHs, OPAHs, APAHs, and MPAHs have demonstrated mutagenic effects and genotoxicity, pointing towards their toxicological significance to human health, though they are typically found at lower concentrations than the analogous UnSubPAHs by 1–2 orders of magnitude (Vincenti et al. 1996; Bezabeh et al. 1997; Bhatia et al. 1998; Layshock et al. 2010; Huang et al. 2013). Their lower concentrations compared to UnSubPAHs make them more difficult to measure and quantify. They can also be more difficult to measure with off-line methods, because they are more easily changed or lost during extraction. For these reasons, understanding the formation, transformation, and impacts of functionalized PAHs lags behind our understanding of the UnSubPAHs.

1.1. Approaches for Measuring Particle-Phase PAHs

Detection of particle-bound PAHs has most commonly been accomplished through off-line analytical procedures (Polidori et al. 2008), collecting samples on filters for later extraction and analysis. The main advantage to off-line techniques has been their ability to both quantify and speciate PAH compounds, discerning even isomers having the same molecular mass. However, off-line approaches also have a major disadvantage in that either high sample concentrations or long averaging times are necessary to collect adequate mass for analysis. This long-term averaging can mask any short-term variability in concentrations. Sampling artifacts are additional risks, such as from evaporation or chemical reactions during long sample times or from the extraction processes. An in-depth discussion of off-line aerosol characterization techniques can be found in the review by Pratt and Prather (2011).

On-line PAH measurement techniques offer the advantage of higher temporal resolution data, allowing the examination of chemical changes in atmospheric aerosol populations on short time or spatial scales. Several approaches for accomplishing this have been described previously, including using the commercial photoelectric aerosol sensor (PAS) (Marr et al. 2004), the aerosol time-of-flight mass spectrometer (ATOFMS) (Silva and Prather 2000), and both the quadrupole aerosol mass spectrometer (Q-AMS) (Džepina et al. 2007) and the newer high-resolution time-of-flight aerosol mass spectrometer (HR-AMS) from Aerodyne Research, Inc. (Billerica, MA) (DeCarlo et al. 2006; Canagaratna et al. 2007). Within on-line PAH measurement techniques, systems that have the capability of identifying unique ions at the same unit mass have advantages over systems that cannot make these distinctions. For example, the HR-AMS separates ions with a typical *m/z* resolving power of 0.01 (meaning the HR-AMS can resolve between peaks with mass-to-charges of 0.01 apart), which enables distinguishing between, for example, the molecular ions for methyl-fluorene $C_{14}H_{12}^{+}$ (exact mass 180.245) and fluorenone $C_{13}H_8O^{+}$ (exact mass 180.202), both with unit *m/z* 180. However, the HR-AMS still cannot distinguish structural differences at the same ion exact mass. Furthermore, even with state-of-the-art on-line technology, it

is still necessary to understand the fragmentation behavior of PAH molecules and the fragmentation behavior of the surrounding particle phase constituents to effectively quantify PAH concentrations.

This article describes a new method for a real-time characterization of the contributions of individual PAH isomers in the aerosol phase. The potential of the method is evaluated using measurements from engine exhaust chamber studies made with an Aerodyne HR-AMS. Using high-resolution analysis, it was possible to isolate and quantify signals from the molecular ions associated with 53 PAH compounds. We describe the procedures for applying this new approach, which depends on resolving ion signals associated with PAHs between *m/z* 128 and *m/z* 279. We also evaluate the potential for interferences from other PAHs and non-PAH organic fragments at the target masses. The results suggest that robust quantification of PAH isomers will be possible by this approach once more complete PAH fragmentation data are available for the HR-AMS. Examining the molecular ion data reveals a high quality time series that allows the particle-phase PAH trends to be determined relative to total organic mass based on individual ions and ion subgroups. The trends observed are in some ways consistent with previous results, but also reveal areas where further focused work will be required.

2. EXPERIMENTAL DATASET

The data used in this analysis were collected during a three-week campaign at the Lovelace Respiratory Research Institute (LRRI) in Albuquerque, NM in April-May 2012. LRRI has a facility capable of operating diesel and gasoline engines under varying conditions and blending their exhaust together in controlled proportions (MacDonald et al. 2003, 2004a,b, 2005, 2011). The major objective of the LRRI campaign was to obtain detailed characterizations of the particle- and gas-phase compositions of the blended exhaust for a wide range of PM loading and engine operating conditions. During the campaign, exhaust from a single diesel generator and a single gasoline engine were sampled under varying operating conditions, mixing ratios, and dilutions. Details of the facility operation and the experiments used in our analysis are included in the online supplemental information, with the experimental conditions provided in Table S1.

2.1. HR-AMS Operation

Particle composition was characterized using an Aerodyne HR-AMS (DeCarlo et al. 2006; Canagaratna et al. 2007). The instrument can quantitatively measure chemically resolved size distributions and bulk mass concentrations of nonrefractory chemical species (including organic and inorganic components) within the aerosol ensemble by alternating between mass spectrum (MS) scanning and particle time of flight (pToF) modes (Allan et al. 2003a; Jimenez et al. 2003). The ToF mass analyzer can operate under two modes (V and W) to provide different traveling distances for the ions, resulting in different sensitivities (~0.003 μg m^{-3} and 0.05 μg m^{-3}, respectively, for nitrate typically) and mass resolving powers (~2000 m/Δm and ~4000 m/Δm, respectively) (DeCarlo et al. 2006).

The HR-AMS collected data with 1-min time resolution at a vaporizer temperature of 600°C, alternating between MS and pToF modes, while the ToF was operated in both V- and W-mode. For each measurement cycle, the system began with V-mode sampling, spending 10 s in MS mode followed by 20 s in pToF mode, and then sampled in W-mode for 30 s in MS mode. Only MS mode data are used in this analysis. The *m/z* range was from 6–1993 in V-mode and 2–330 in W-mode. The average resolution at *m/z* 28 was 2900 and 4000 in V- and W-modes, respectively. At *m/z* 32, the average resolution was 3400 and 4000 in V- and W-mode, respectively, and at *m/z* 184, the average resolution was 3500 and 4000 in V- and W-mode, respectively. Both V- and W-mode data were used to identify ions in the HR data and to compare overall concentrations; however, only the V-mode data are presented here. All data from the HR-AMS were analyzed using SQUIRREL (version 1.55), and the high-resolution analysis software tool, PIKA (version 1.14) (Sueper 2010). Flow, mass accuracy, velocity, and ionization efficiency (IE) calibrations were performed following standard procedures. Mass accuracy (i.e., *m/z*) calibrations included multiple tungsten isotopes (*m/z* 181.95, 183.95, and 185.95) that appear in HR-AMS mass spectra as an instrument artifact. The inclusion of these ions in the *m/z* calibration allows accurate attribution of ions at the higher masses relevant for PAH analysis.

Consistent with common practice, we used the fragmentation algorithm described by Allan et al. (2004). Gas-phase corrections to the standard fragmentation table were done based on HEPA filtered air sampled from the inlet line. In addition, the CO_2^+ signal was corrected using real-time CO_2 gas-phase concentrations measured using a Li-Cor closed path CO_2/H_2O analyzer. During the study CO_2 concentrations averaged 4,200 ppm and went as high as 21,500 ppm. The AMS measured inlet flow was corrected to standard temperature and pressure. The single ion (SI) value in both V- and W-mode were documented during the campaign and the values were postcorrected during data analysis. Common practices were used to postcorrect the air beam (AB) to account for natural drift in the instrument sensitivity (Allan et al. 2003b). As recommended by Timko et al. (2009, 2014), we have also removed signal contributions related to the contamination artifacts that arise from the fragmentation of aerosolized polydimethylsiloxane ($SiO(CH_3)_2$), found in conductive silicone tubing.

As with several prior engine exhaust studies using an AMS (Canagaratna et al. 2004; Slowik et al. 2004; Matthew et al. 2008; Chirico et al. 2010; Dallmann et al. 2014), a collection efficiency (CE) of unity was used to estimate the aerosol mass concentration for all experiments. Studies using an HR-AMS

to quantify PAHs in wood combustion studies have also used CE = 1 (Eriksson et al. 2014; Bruns et al. 2015a). Any uncertainty associated with the choice of CE would affect the absolute concentrations of particulate components, but would not affect the relative quantities or the mass spectral features. Furthermore, Organic (Org), nitrate (NO_3), sulfate (SO_4), ammonium (NH_4), and chloride (Chl) concentrations have been quantified based on the relative ionization efficiency (RIE) of individual species. PAH-associated ions are treated similarly to all other Org species using an RIE of 1.4. Džepina et al. (2007) and Slowik et al. (2004) each tested four PAH standards and found RIEs ranging between 1.35 and 2.1.

The detection limits (DLs) of the five major nonrefractive species (Org, NO_3, SO_4, NH_4, and Chl) and of the PAH family of ions were determined from filter samples taken at the beginning and end of sampling each chamber experiment. Test04 is an exception; in this test a filter sample was only taken in the middle of the experiment, leading to inaccurate DLs due to the shorter filter sampling time and the high PM loading. Each detection limit was calculated as three times the standard deviation of high-resolution filter sample concentrations. Table S2 (see the supplementary information) summarizes the DLs (in μg m^{-3}) using 30-s sampling times.

Elemental analysis (EA) was performed using the recently updated calibration factors described by Canagaratna et al. (2015). EA has been shown to be useful in obtaining the average elemental composition in organic aerosols thus allowing for a more accurate calculation of the density of the organic material (Kuwata et al. 2012). The calculated density of organic material was determined to be smaller than the frequently assumed 1.2 g cm^{-3}; values ranged between 0.85 and 1.1 g cm^{-3} depending on test conditions.

2.2. Supporting Instrumentation

Additional particle-phase measurements complemented the HR-AMS data. The total particle mass was collected on 47-mm Pallflex (Pall-Gelman, East Hills, NY) filters, then measured gravimetrically during each chamber experiment with a Mettler MT5 microbalance located in the exposure laboratory. Total PAHs adsorbed onto the particle surfaces (ng m^{-3}) were measured with a PAS 2000CE. The PAS is factory-calibrated for surface PAH concentrations up to 1000 ng m^{-3} and expected to give a linear response up to 5000 ng m^{-3}. The manufacturer-reported limit of detection for the PAS is 10 ng m^{-3} and Marr et al. (2004, 2006) has previously estimated uncertainty with the PAS as 20%.

CO_2 and water vapor concentrations were measured using a Li-Cor 840A analyzer. Factory response factors were used to calculate CO_2 and water vapor mixing ratios, with the instrument performance for CO_2 also verified by using a calibration gas containing 390 ppmv CO_2 ± 1% (Scott Marrin). CO_2 and water vapor concentrations were recorded at 1 Hz and then time averaged to 1 min.

3. QUANTIFICATION OF PAHS BY MOLECULAR ION PROXY (P-MIP)

3.1. Fragmentation of PAHs in the HR-AMS

An examination of the HR-AMS spectra obtained during the LRRI experiments revealed peaks at masses consistent with the ionization of PAH molecules. These ions were not generally included in the existing PIKA database, which extends only to *m/z* 120, but their presence in AMS mass spectra has been previously observed in some limited cases. In one of the earliest papers characterizing AMS instrument performance, Alfarra (2004) compared mass spectra from a Q-AMS against those reported by NIST for a wide range of compounds, including pyrene, a PAH with MW = 202. For pyrene, Alfarra found that smaller ion fragments (< *m/z* 60) were relatively more intense in the AMS spectra, while higher masses were relatively less intense. He concluded that the AMS vaporization/ionization configuration results in a more significant fragmentation of long chain species than in standard EI ionization mass spectrometry. However, both the NIST and Q-AMS spectra had *m/z* 202 as the most significant fragment contribution for pyrene; for the Q-AMS the relative abundance of *m/z* 202 to the total signal was 27% while in the NIST spectra it was 53%.

Džepina et al. (2007) tested eight additional PAH standards with molecular weights between 202 and 300 using the Q-AMS. The tested compounds were pyrene ($C_{16}H_{10}$, MW = 202), 1-methylpyrene ($C_{17}H_{12}$, MW = 216), 2,3-benzofluorene ($C_{17}H_{12}$, MW = 216), triphenylene ($C_{18}H_{12}$, MW = 228), 10-methylbenz [a]anthracene ($C_{19}H_{14}$, MW = 242), benzo[e]pyrene ($C_{20}H_{12}$, MW = 252), benzo[ghi]perylene ($C_{22}H_{12}$, MW = 276), and coronene ($C_{24}H_{12}$ MW = 300). In each case but one (2,3-benzofluorene), the highest contributing ion in the mass spectra was associated with the molecular ion, accounting for between 20% and 36% of the total mass signal. This finding was consistent with prior studies of EI ionization, which found that 20% of the abundance of the PAH molecular signal is associated with the molecular ion (Lee et al. 1981). Both 1-methylpyrene and 2,3-benzofluorene are odd-PAHs (o-PAHs), having an odd number of carbon atoms. This structure leads to reduced stability during ionization. Džepina (2007) and her coauthors observed that for each o-PAH analyzed by the Q-AMS, a major contributing ion occurred at the $[M\text{-}H]^+$ ion. While the relative contributions of the molecular ions did vary, PAH mass spectra generally consisted of an intense molecular ion peak, smaller peaks at ions due to the loss of one to four hydrogen atoms, and doubly charged ions. Dzepina and her coauthors also developed a method for quantifying PAHs in ambient sample that depended on inferred fragmentation patterns in the UMR mass spectra. However, later work revealed several instances where there were significant errors in the inferred fragmentation patterns (Eriksson et al. 2014), and this PAH quantification approach has not been broadly adopted.

Aiken et al. (2007) measured three PAHs using the higher resolution W-mode in a HR-AMS – pyrene ($C_{16}H_{10}$, MW = 202), fluoranthene ($C_{16}H_{10}$, MW = 202), and benzo[e]pyrene

($C_{20}H_{12}$, MW = 252) – and found good correlation between the HR-AMS and NIST spectra. They showed that the strongest signal in the spectra occurred at the molecular ion mass in all three cases: 18.0% of the relative signal for fluoranthene, 49.6% for pyrene, and 17.8% for benzo[e]pyrene.

Most recently, a HR-AMS was used to quantify 18 PAH "base ions" (Bruns et al. 2015b), generated during wood burning and then oxidized to form secondary organic aerosol (SOA). These base ions, denoted as [M], are treated as PAH molecular ions but the parent molecule is not always identified. Bruns and colleagues used the high-resolution mass spectral data to determine ratios between their PAH base ion and each of its "associated ions" in the primary emissions (measured before photooxidation). The analyzed associated ions included signals from $[M]^{2+}$, $[M-H]^{+}$, $[M-H]^{2+}$, $[M-2H]^{+}$, $[M+H]^{+}$, and $[M+H]^{2+}$ (where M is the mass of the base ion and H is the mass of a hydrogen atom), as well as the isotopic contributions from each of the singly charged ions from the presence of a single ^{13}C. The mechanism for how the addition of hydrogen atoms to form $[M+H]^{+}$ or $[M+2H]^{+}$ ions occurs in the HR-AMS is not explained in the article. The ratios of each associated ion to base ion signal were derived from the primary emissions of a single high load experiment and were then incorporated into the UMR fragmentation table (associated ion signal = ratio value/base ion signal) and applied to the entire dataset.

3.2. P-MIP Procedure

Building on this previous body of work, we develop here a new approach for analyzing HR-AMS data to quantify PAHs, using the PAH molecular ions as a proxy (P-MIP). The P-MIP analysis will not in itself allow for the direct quantification of each PAH species unless standard mass spectra are available for each compound, a step left for future work. However, even in the absence of PAH standard spectra, P-MIP is still useful for tracking the relative presence of different PAH species within a sample.

P-MIP analysis depends first on identifying target molecular ions for PAH species within the mass spectra. To isolate the contributions of specific PAH-related ions in the observed signal, a list of target molecular ions was developed from three sets of sources: (1) PAH-related molecular ions that have been identified in previous AMS measurement studies (Alfarra 2004; Aiken et al. 2007; Džepina et al. 2007); (2) PAHs that have been prominently linked to diesel emissions (Frenich et al. 2010; Pandey et al. 2011; Alkurdi et al. 2013; Huang et al. 2013) or to particularly strong health impacts (US EPA 1992; International Agency for Research 2013); and (3) PAHs that are consistent with ions that are prominent in one or more mass spectra from the LRRI case study experiments. Table 1 lists the 53 target PAHs identified by this process, which include molecular ions from 15 UnSubPAHs, 12 MPAHs, 15 OPAHs, 7 NPAHs, and 4 APAHs. The identified PAHs range from two to six rings and have mass-to-charge ratios (*m/z*) between 128 and 279.

After the molecular ion for each target PAH was identified in the HR signal, it was next necessary to further identify surrounding ion masses that were not initially included in the standard PIKA ion-fitting list. The identification of unknown ion formulas was initiated using the fragmentation patterns of higher molecular-weight PAHs, alkanes, hopanes, steranes, and other cyclic compounds typically generated in engine exhaust as structural starting points for ion signal identification at smaller *m/z*. For example, when the molecular ion could be clearly identified in the HR signal for nitrochrysene ($C_{18}H_{11}NO_2^{+}$) at *m/z* 273, then related signals would also be present at, e.g., *m/z* 227 $[M-46]^{+}$ after loss of NO_2, at *m/z* 226 $[M-47]^{+}$ after loss of HNO_2, and at *m/z* 216 $[M-58]^{+}$ after loss of CNO_2. Following this progression of fragment identification for each of the target PAHs, as well as for other large molecules identified in engine exhaust, allowed for realistic resolution of the signal. This approach identified the most appropriate and realistic ions in engine exhaust. A web-based tool (www.chemcals.com) provided a second complementary ion identification step (Patiny and Borel 2013), by aiding the identification of additional ions located in the HR-AMS signal spectrum. Combining these approaches, a total of 2488 ions (1030 dominant ions and 1458 less dominant isotopes) were fit and identified in the HR mass spectra out to *m/z* 279. The 1458 less dominant isotopes were constrained by assigning their abundance based on the theoretical value relative to the dominant isotope ion. After completing the fits, mass spectral residuals were 5% or less for all available LRRI data. Molecular ions for PAHs larger than *m/z* 279 could also be identified in the HR mass spectra; however, the large number of possible molecular formulas at these *m/z* made it difficult to robustly resolve the surrounding ions, and so they were omitted from the analysis. For the LRRI data set, on average only 0.06% of the aerosol mass signal occurred above *m/z 279*; the range for individual tests was 0.04–0.21%.

In applying P-MIP analysis, the distinction must be maintained between PAH molecular ion concentrations ($C_{\mathrm{ion},i}$, $C_{\mathrm{ion,C10H8}}$, $C_{\mathrm{ion,C11H8}}$, etc.) and PAH compound concentrations (C_i, C_{C10H8}, C_{C11H8}, etc.) with respect to the HR-AMS measurements. Here, $C_{\mathrm{ion},i}$ refers to the molecular ion associated with each of the PAHs (such as those listed in Table 1). The PAH compound concentrations (C_i) can be approximated based on the relative abundance ($f_{A,i}$) of the PAH molecular ion in reference mass spectra (obtained for single PAH compounds). Thus the total concentration for any PAH compounds is calculated as follows:

$$C_i = \frac{C_{\mathrm{ion},i}}{f_{A_i}} \quad [1]$$

It is critical to note that for most of the PAHs, including those in this study, standard mass spectra have not yet been

TABLE 1
List of 53 target PAH compounds for P-MIP analysis. This list includes 15 UnSubPAH ions, 15 OPAH ions, 12 MPAH ions, 7 NPAH ions, and 4 APAH ions. In the cases of *m/z* 156, 168, 180, 182, 194, and 256 the exact mass of the two molecular ions are unique and can be independently identified in the AMS signal

m/z	Molecular Formula	Common Name	Category	# Rings
128	$C_{10}H_8$	Naphthalene	UnSubPAH	2
152	$C_{12}H_8$	Acenaphthylene	UnSubPAH	3
154	$C_{12}H_{10}$	Acenaphthene	UnSubPAH	3
166	$C_{13}H_{10}$	Fluorene	UnSubPAH	3
176	$C_{14}H_8$	Paracyclene	UnSubPAH	4
178	$C_{14}H_{10}$	Anthracene	UnSubPAH	3
		Phenathrene		
190	$C_{15}H_{10}$	Benzo[def]fluorene	UnSubPAH	4
202	$C_{16}H_{10}$	Pyrene	UnSubPAH	4
		Fluoranthene		
		Acephenanthrylene		
216[a]	$C_{17}H_{12}$	Benzofluorene	UnSubPAH	4
		Methylpyrene	MPAH	4
226	$C_{18}H_{10}$	Cyclopenta[cd]pyrene	UnSubPAH	5
		Benzo[ghi]fluoranthene		
228	$C_{18}H_{12}$	Benz[a]anthracene	UnSubPAH	4
		Triphenylene		
		Chrysene		
250	$C_{20}H_{10}$	Corannulene	UnSubPAH	6
		Dicyclopenta[cd,mn]pyrene		
252	$C_{20}H_{12}$	Benzo[b]fluoranthene	UnSubPAH	5
		Benzo[j]fluoranthene		
		Benzo[k]fluoranthene		
		Benzo[a]pyrene		
		Benzo[e]pyrene		
276	$C_{22}H_{12}$	Indio[1,2,3-cd]pyrene	UnSubPAH	6
		Benzo[ghi]perylene		
278	$C_{22}H_{14}$	Dibenzanthracene	UnSubPAH	5
		Pentacene		
142	$C_{11}H_{10}$	Methyl-naphthalene	MPAH	2
156	$C_{12}H_{12}$	Dimethyl-naphthalene	MPAH	2
168	$C_{13}H_{12}$	Methyl-acenaphthene	MPAH	3
180	$C_{14}H_{12}$	Methyl-fluorene	MPAH	3
192	$C_{15}H_{12}$	Methyl-phenanthrene	MPAH	3
194	$C_{15}H_{14}$	Dimethyl-fluorene	MPAH	3
206	$C_{16}H_{14}$	Ethyl-phenathrene	MPAH	3
220	$C_{17}H_{16}$	Trimethyl-phenanthrene	MPAH	3
234	$C_{18}H_{18}$	Retene	MPAH	3
		Tetramethyl phenanthrene		
242	$C_{19}H_{14}$	Methylbenz[a]anthracene	MPAH	4
		methyl chrysene		
256	$C_{20}H_{16}$	Di-methylbenz(a)anthracene	MPAH	4
268	$C_{21}H_{16}$	Methyl cholanthrene	MPAH	5
132	C_9H_8O	Indanone	OPAH	2
156	$C_{11}H_8O$	Benzocycloheptenone	OPAH	2

(*Continued on next page*)

TABLE 1
List of 53 target PAH compounds for P-MIP analysis. This list includes 15 UnSubPAH ions, 15 OPAH ions, 12 MPAH ions, 7 NPAH ions, and 4 APAH ions. In the cases of *m/z* 156, 168, 180, 182, 194, and 256 the exact mass of the two molecular ions are unique and can be independently identified in the AMS signal *(Continued)*

m/z	Molecular Formula	Common Name	Category	# Rings
158	$C_{10}H_6O_2$	Naphthoquinone	OPAH	2
168	$C_{12}H_8O$	Dibenzofuran	OPAH	3
180	$C_{13}H_8O$	Fluorenone	OPAH	3
182	$C_{13}H_{10}O$	Dibenzopyran	OPAH	3
182	$C_{12}H_6O_2$	Acenaphthoquinone	OPAH	3
184	$C_{12}H_8O_2$	Hydroxydibenzofuran	OPAH	3
194	$C_{14}H_{10}O$	Anthrone	OPAH	3
196	$C_{13}H_8O_2$	Xanthone	OPAH	3
204	$C_{15}H_8O$	Cyclcopenta-phenanthrene-one	OPAH	4
208	$C_{14}H_8O_2$	Anthraquinone	OPAH	3
232	$C_{16}H_8O_2$	Aceanthraquinone	OPAH	4
254	$C_{19}H_{10}O$	Benzo[cd]pyrenone	OPAH	5
258	$C_{18}H_{10}O_2$	Benzanthracene	OPAH	4
173	$C_{10}H_7NO_2$	Nitro-naphthalene	NPAH	2
199	$C_{12}H_9NO_2$	Nitro-acenaphthlene	NPAH	3
211	$C_{13}H_9NO_2$	Nitro-fluorene	NPAH	3
223	$C_{14}H_9NO_2$	Nitro-anthracene Nitro-phenathrene	NPAH	3
247	$C_{16}H_9NO_2$	Nitro-pyrene	NPAH	4
256	$C_{13}H_8N_2O_4$	Dinitrofluorene	NPAH	3
273	$C_{18}H_{11}NO_2$	Nitrochrysene	NPAH	4
217	$C_{16}H_{11}N$	Aminopyrene Carbazole	APAH	4
259	$C_{18}H_{13}NO$	Aminobenzanthrone	APAH	4
267	$C_{20}H_{13}N$	Dibenzocarbazole Amino benzopyrene	APAH	5
279	$C_{21}H_{13}N$	Dibenz[a,j]acridine	APAH	5

[a]At m/z 216 the UnSubPAH and MPAH have identical exact masses and cannot be independently identified.

measured using an HR-AMS or other comparable vaporization/ionization technology. Thus the relative abundance coefficients ($f_{A,i}$) cannot yet be determined for most PAHs. However, there are a few laboratory-measured standard spectra using the AMS; spectra measured by Džepina et al. (2007), Aiken et al. (2007), and Alfarra (2004) are available on the public AMS mass spectral database (Ulbrich et al. 2007; Ulbrich et al. 2009). The sampled PAHs include pyrene ($C_{16}H_{10}$, *m/z* 202), fluoranthene ($C_{16}H_{10}$, *m/z* 202), 2,3-benzofluorene ($C_{17}H_{12}$, *m/z* 216), 1-methylpyrene ($C_{17}H_{12}$, *m/z* 216), triphenylene ($C_{18}H_{12}$, *m/z* 228), 10-methylbenz[a]anthracene ($C_{19}H_{14}$, *m/z* 242), benzo[e]pyrene ($C_{20}H_{12}$, *m/z* 252), and benzo[ghi]perylene ($C_{22}H_{12}$, *m/z* 276). For these compounds, the relative contribution of the molecular ion to the total mass spectrum ranged from 17% to 37%. Table 2 lists the relative abundance of the molecular ion for each previously characterized PAH compound.

Equation (1) and the definitions of C_i and $C_{\text{ion},i}$ are appropriate for individual compounds. A similar distinction should be made for the summed category PAH molecular ion concentrations ($\text{PAH}_{\text{ion total}}$, $\text{OPAH}_{\text{ion total}}$, $\text{UnSubPAH}_{\text{ion total}}$, etc.) and PAH concentrations ($\text{PAH}_{\text{total}}$, $\text{OPAH}_{\text{total}}$, $\text{UnSubPAH}_{\text{total}}$, etc.). For example, the total molecular ion concentration associated with OPAH, using the species included in this study, is calculated as:

$$\begin{aligned}\text{OPAH}_{\text{ion total}} = \sum_{\text{OPAH}_i} C_{\text{ion,i}} = {} & C_{\text{ion},C_9H_8O} + C_{\text{ion},C_{11}H_8O} \\ & + C_{\text{ion},C_{10}H_6O_2} + C_{\text{ion},C_{12}H_8O} + C_{\text{ion},C_{13}H_8O} \\ & + C_{\text{ion},C_{13}H_{10}O} + C_{\text{ion},C_{12}H_6O_2} + C_{\text{ion},C_{12}H_8O_2} \\ & + C_{\text{ion},C_{14}H_{10}O} + C_{\text{ion},C_{13}H_8O_2} + C_{\text{ion},C_{15}H_8O} \\ & + C_{\text{ion},C_{14}H_8O_2} + C_{\text{ion},C_{16}H_8O_2} + C_{\text{ion},C_{19}H_{10}O} \\ & + C_{\text{ion},C_{18}H_{10}O_2}\end{aligned} \quad [2]$$

TABLE 2
Relative abundance ($f_{A,i}$) of PAH signal at the molecular ion mass based on AMS laboratory PAH standards. Spectra data are obtained from AMS spectra database Ulbrich et al. (2007) and refer to original publications by (1) Džepina et al. (2007); (2) Aiken et al. (2007); and (3) Alfarra (2004)

m/z	Molecular Formula	Common Name	Relative Abundance at Molecular Ion Mass
202	$C_{16}H_{10}$	Pyrene	0.363[1]
			0.372[2]
			0.271[3]
202	$C_{16}H_{10}$	Fluoranthene	0.321[2]
216	$C_{17}H_{12}$	Benzofluorene	0.268[1]
216	$C_{17}H_{12}$	Methylpyrene	0.198[1]
228	$C_{18}H_{12}$	Triphenylene	0.259[1]
242	$C_{19}H_{14}$	Methylbenz[a]anthracene	0.170[1]
252	$C_{20}H_{12}$	Benzo[b,j,k]fluoranthene	0.262[1]
			0.256[2]
276	$C_{22}H_{12}$	Benzoperylene	0.244[1]
300	$C_{24}H_{12}$	Coronene	0.206[1]

While the total OPAH associated concentration is calculated as:

$$\mathrm{OPAH_{total}} = \sum_{\mathrm{OPAH}_i} \frac{C_{\mathrm{ion},i}}{f_{A_i}} = \sum_{\mathrm{OPAH}_i} C_i = C_{C_9H_8O} + C_{C_{11}H_8O} + C_{C_{10}H_6O_2} + C_{C_{12}H_8O} + C_{C_{13}H_8O} + C_{C_{13}H_{10}O} + C_{C_{12}H_6O_2} + C_{C_{12}H_8O_2} + C_{C_{14}H_{10}O} + C_{C_{13}H_8O_2} + C_{C_{15}H_8O} + C_{C_{14}H_8O_2} + C_{C_{16}H_8O_2} + C_{C_{19}H_{10}O} + C_{C_{18}H_{10}O_2} \quad [3]$$

Equations for each of the other subgroups can be derived similarly.

3.3. PAH Molecular Ion Signal Interference Considerations

The effectiveness of the P-MIP analysis for quantifying the contributions of individual PAH compounds is impacted by the degree to which other compounds interfere with the molecular ion signals. Such interferences could come either from non-PAH species, including isotopic ions, or from other PAHs. A first step toward evaluating potential interferences is to determine what classes of competing compounds may be present. For engine exhaust, the broad array of potential chemical constituents has been characterized in previous studies (Rogge et al. 1993; Fraser et al. 1998; Schauer et al. 1999, 2002; He et al. 2006). Based on these studies, which reported both the gas- and particle-phase emissions of organic compounds in the exhaust, the predominant large non-PAH organic compounds in the particle phase were n-alkanes (C_{18}-C_{29}), branched alkanes (C_{15}-C_{18}), saturated cycloalkanes, hopanes, steranes, n-alkanoic acids, alkanedioic acids, and aromatic acids. Fortunately, our assessment indicates that the ions associated with each of these major competing compound classes are distinct from the set of PAH molecular ions. This finding was reached by first identifying fragmentation patterns for each of the competing compound classes through repeated analysis of individual compounds within a single compound class. Next, any ion fragments appearing with the same unit mass as our target PAHs were inspected for exact chemical structure. From this analysis of over two-dozen compounds a trend developed that the non-PAH ion fragments that occurred at the same unit *m/z* consistently had H:C ratios greater than one, whereas the PAH molecular ions had H:C ratios that were less than or equal to one (cf. Table 1). This finding parallels a prior argument by Canagaratna et al. (2004) and is supported by previous studies of the fragmentation patterns of alkanes, alkenes, and aromatics (Mohr et al. 2009) and of aromatics (Tobias et al. 2001). The resolution of the HR-AMS is such that the PAH molecular ions' signals can be unambiguously distinguished from those of ions associated with non-PAH sources.

Another class of potential interferents on the PAH molecular ions are non-PAH ^{13}C isotope ions. A survey of the HR signals of all 53 PAH molecular ions showed such ions were present as very near neighbors for 14 of 15 UnSubPAHs and 9 of 12 MPAHs; instances can be seen in Figure 1. Three MPAH and one UnSubPAH molecular ions had no overlapping ^{13}C isotopic ions (at *m/z* 234, 256, 268, and 276), nor did any of the NPAH, OPAH, or APAH molecular ions. Fortunately, the abundances of the ^{13}C isotopic ions are well constrained, and algorithms are already in place within PIKA to fit them based on the fit of the more abundant ^{12}C isotope and

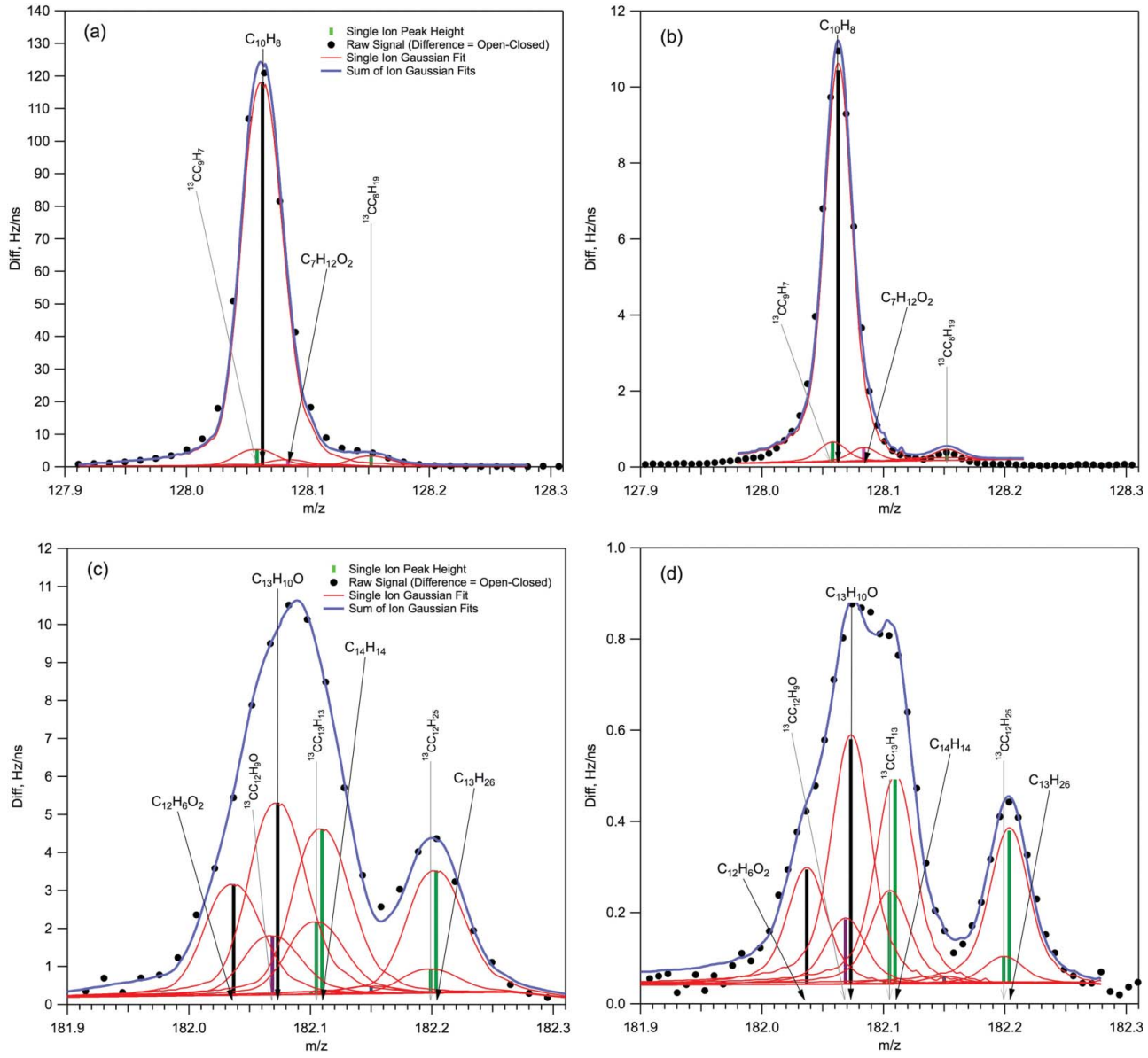

FIG. 1. Examples of the HR-AMS high-resolution ion fitting from LRRI Test04 from *m/z* 128 and *m/z* 182 in both V- and W-mode. PAH ions of interest are $C_{12}H_8$ at *m/z* 128 and for $C_{12}H_8O$ and $C_{13}H_{10}O$ at *m/z* 182. (a) V-mode ion fits for *m/z* 128; (b) W-mode ion fits for *m/z* 128; (c) V-mode ion fits for *m/z* 182; (d) W-mode ion fits for *m/z* 182.

their relative abundance. In these cases the error of the isotope ion is therefore also predetermined by the signal of the parent ion and the relative isotopic abundance and does not depend on the signal at the *m/z* of the isotopic ion (Sueper 2014). The presence of near-neighbor isotopic ions increases the uncertainty in the fit of the target PAH molecular ion, but the uncertainty remains well-defined. These errors will be evaluated for the LRRI data set later in the article.

A more significant source of potential interferences in the P-MIP analysis are those arising from fragments of larger PAH molecules, as these are less easily constrained. One example from prior studies is benzo[e]pyrene ($C_{20}H_{12}$, *m/z* 252). As shown by Aiken et al. (2007) and Džepina et al. (2007), benzo[e]pyrene can fragment during the vaporization/ionization process to produce a fragment ion of identical empirical formula to that of the pyrene molecular ion ($C_{16}H_{10}^+$, *m/z* 202). If both benzo[e]pyrene and pyrene are present in a sample, then the observed signal at *m/z* 202 for $C_{16}H_{10}^+$ would be partially due to pyrene and partially due to fragments originating from benzo[e]pyrene. Fortunately, an inspection of the fragmentation patterns from previously studied PAH laboratory standards, using a Q-AMS (Alfarra 2004; Džepina et al. 2007) and HR-AMS (Aiken et al. 2007), shows that such interferences are usually small. Table S3 (see the

supplemental information) lists the contributions to the molecular ion signals of PAHs listed in Table 1 from the nine PAH compounds that have available laboratory AMS spectra. Typically, the fraction of a PAH's signal that overlaps with another smaller PAH's molecular ion ranges between 0.005% and 1.2% of the total signal. At these levels, the interference of the larger PAH onto the smaller would result in only a small bias.

EI spectra for most other PAH compounds are available from the NIST database (NIST Mass Spec Data Center 2014), and it is tempting to use these spectra to attempt to further probe the PAH fractionation patterns and potential interferences in the HR-AMS. However, it is not appropriate to apply NIST reference spectra to P-MIP analysis; the HR-AMS vaporization/ionization process usually results in significantly greater fragmentation than other EI techniques included in NIST database (Figure S2, see the supplemental information). There is even some evidence that fragmentation patterns may vary between individual AMS instruments. Three independent measurements are available for the fragmentation of a laboratory standard of pyrene (Alfarra 2004; Aiken et al. 2007; Džepina et al. 2007). In comparing these three measurements, the fractional signal contributions at the molecular ion mass (*m/z* 202) were observed to be 36%, 37%, and 27% by Džepina et al. (2007), Aiken et al. (2007), and Alfarra (2004), respectively, while the contributions at other fragment ion masses along the spectra are comparable. The smaller signal observed by Alfarra at the molecular ion occurred despite the fact the AMS in his study was operated at a lower vaporizer temperature, 500–550°C, versus 600°C for the other two studies. In another instance where two different measurements of the same PAH compound yielded different results, Aiken et al. (2007) observed a 6% contribution from benzo[e]pyrene at *m/z* 202 (due to fragmentation), a <0.1% contribution at *m/z* 216, and a 26% contribution at *m/z* 252, while Džepina et al. (2007) found the contributions from the same PAH compound to be 0.8%, 0.8%, and 26%, for *m/z* 202, 216, and 252, respectively. All of these results are included in Table S3 (see the supplemental information). Differences in instrument tuning are a likely cause for these variations in performance.

There are specific circumstances where the interferences from larger PAHs onto the signals of smaller PAH molecular ions are likely to be particularly significant – when the two PAH compounds are separated by 2 amu. The $[M\text{-}2H]^+$ ion is frequently a major fragment in EI mass spectra for PAHs, as previously reported by Džepina et al. (2007). Two such cases exist for PAHs where Q-AMS or HR-AMS standard spectra are available – one where a fragment of $C_{18}H_{12}$ (triphenylene and its isomers, *m/z* 228) affects the signal associated with the molecular ion $C_{18}H_{10}^+$ (cyclopenta[cd]pyrene and its isomers, *m/z* 226), and another where a fragment from benzo[e]pyrene ($C_{20}H_{12}$, *m/z* 252) interferes with the molecular ion $C_{20}H_{10}^+$ (corannulene and its isomers, *m/z* 250). In these cases, the fragmentation pattern of triphenylene and benzo[e]pyrene show that ~10% of their total signal is found at the $[M\text{-}2H]^+$ fragment, corresponding to the $C_{18}H_{10}^+$ and $C_{20}H_{10}^+$ ions, respectively. These same ion masses also remain present as the molecular ions for their respective PAH compounds. While the available compounds with AMS-measured laboratory standards are limited, the same interference pattern is likely to be seen for seven additional PAH pairs among the compounds included in this study – $C_{12}H_{10}$ (acenaphthene, *m/z* 154) with the $C_{12}H_8^+$ (acenaphthylene, *m/z* 152) ion, $C_{12}H_{12}$ (dimethylnapthalene, *m/z* 156) with the $C_{12}H_{10}^+$ (acenaphthene, *m/z* 154) ion, $C_{13}H_{12}$ (methyl-acenaphthene, *m/z* 168) with the $C_{13}H_{10}^+$ (fluorene, *m/z* 156) ion, $C_{14}H_{10}$ (anthracene and its isomers, *m/z* 178) with the $C_{14}H_8^+$ (paracyclene, *m/z* 176) ion, $C_{15}H_{12}$ (methyl-phenanthrene, *m/z* 192) with the $C_{15}H_{10}^+$ (benzo[def]fluorene, *m/z* 190) ion, $C_{15}H_{14}$ (dimethyl-fluorene, *m/z* 194) with the $C_{15}H_{12}^+$ (methyl-phenanthrene, *m/z* 192) ion, and $C_{22}H_{14}$ (debenzanthracene and its isomers, *m/z* 278) with the $C_{22}H_{12}^+$ (indio[1,2,3-cd]pyrene and its isomers, *m/z* 176) ion. In these instances, the true signal associated with the smaller PAH's molecular ion is the measured ion signal for that ion minus the calculated contribution from the $[M\text{-}2H]^+$ fragment of the larger PAH's signal (which could be calculated as a fraction of the larger PAH's molecular ion signal). The degree to which these interferences affect the interpretation of the P-MIP analysis depends on the relative amount of the larger and smaller PAHs in each sample; this will be evaluated for the LRRI dataset in section 4.

Mueller et al. (2015) recently described a strategy to quantify PAH ions with the HR-AMS in a way that largely avoids interference issues. Like P-MIP, this alternative approach uses PAH molecular ions as the signal source, but rather than using the dominant ion, it focuses specifically on doubly charged ions that include a single ^{13}C atom. This is an elegant solution to the interference problem, as such ions typically have no near neighbors and can therefore be unambiguously resolved when detectable. However, the doubly-charged ^{13}C isotopic molecular ion is also much less abundant then the dominant molecular ion, by roughly two orders of magnitude (Mueller et al. 2015). Thus only the most concentrated PAHs would be detectable by this approach, making it unlikely to be broadly useful.

4. APPLICATION OF P-MIP ANALYSIS TO ENGINE EXHAUST DATA

We applied the new P-MIP analysis approach to the data set of diesel and gasoline engine exhaust mixtures collected at LRRI in April-May 2012. We first compared these exhaust measurements to AMS mass spectral data available from other groups for diesel and gasoline exhaust. Figure S3 (see the supplemental information) shows the AMS relative abundances from previously published work in comparison with the LRRI data. While the plots suggest some differences that may be attributable to fuel, engine type, or operating conditions, overall the sets of spectra correlate well, with r^2 coefficients

ranging between 0.88 and 0.90. Because the LRRI data are largely representative of gasoline and diesel exhaust primary emissions, it provides a good test data set for the P-MIP analysis procedure. Note that throughout the P-MIP analysis presented here, data are shown for molecular ions only. Standard spectra are not yet available for most PAHs, and therefore $f_{A,I}$ is not known and the parent PAH concentration could not be calculated.

The HR-AMS spectra were resolved between *m/z* 12 and *m/z* 279 using the high-resolution data analysis package PIKA. Figure 1 provides examples of one easily identified UnSubPAH molecular ion, naphthalene ($C_{10}H_8^+$, *m/z* 128), and also two OPAH molecular compounds both located at *m/z* 182, acenaphthoquinone ($C_{12}H_6O_2^+$) and dibenzopyran ($C_{13}H_{10}O^+$). Results for both V-mode and W-mode are provided. For *m/z* 128, the signal is dominated by the naphthalene molecular ion ($C_{10}H_8^+$), with only small signal contributions from the $C_7H_{12}O_2^+$ ion and two isotopic ions, $^{13}CC_9H_7^+$ and $^{13}CC_8H_{19}^+$. In this case, all the ions necessary to accurately fit the signal were already available in the PIKA ion analysis library. However, for the signal at *m/z* 182, the PAH molecular ions $C_{12}H_6O_2^+$ (acenaphthoquinone) and $C_{13}H_{10}O^+$ (dibenzopyran) were not included in the default PIKA library; nor were the other two dominant organic ion fragments, $C_{14}H_{14}^+$ and $C_{13}H_{26}^+$. As in many other cases, it was necessary to add these ions to the PIKA library to complete the analysis.

The P-MIP analysis revealed that prominent PAH features were present in the experiment-average mass spectra throughout the LRRI dataset. One representative example is shown in Figure 2, which shows the entire spectrum (from *m/z* 12–280) with contributions of organics, lumped inorganic components, and PAH molecular ions each indicated. It can be seen in the *m/z* range >100 that the PAH molecular ions are a significant fraction of the HR-AMS signal. Additional data for each of the sixteen tests are reported in Table S4 (see the supplemental information) and include: average mass loadings of Org, NO_3, SO_4, NH_4, and Chl; average summed PAH molecular ions and for each of the subcategories; average elemental ratios for H:C, O:C, and N:C; and the average calculated organic density. The average values are determined from the HR-AMS V-mode time series data as simple averages across the duration of each test. For any summed quantities, the reported value is the average of the summed data. While there were at times significant variations in the measured concentrations during a test, all data were included in the calculated mean values to best capture the average performance of the engines under a given set of operating conditions. Figure 3 demonstrates the temporal variability of Org as a box and whisker plot with the mean and 10th, 25th, 75th, and 90th percentiles for each of the 16 tests shown. The Org concentrations in the set of experiments varied by more than an order of magnitude, providing an opportunity to evaluate the effectiveness of the P-MIP analysis over a similarly broad range of PAH loadings.

Mean values and mean measurement errors were calculated for each of the 53 target PAH isomers for each of the LRRI experiments. Representative results from two tests, Test04 and Test21, are shown in Table S5 (see the supplemental information). Measurement errors were calculated for each measurement time using the procedure included in PIKA, as described by Sueper (2014) and Corbin et al. (2015). For these tests, average measurement errors were 0.0013 ± 0.0008 μg m^{-3} (Test04) and 0.0010 ± 0.0008 μg m^{-3} (Test21). Results for other tests were similar. For less abundant PAH molecular ions, these measurement errors were of the same magnitude as the test-average concentrations. For more abundant ions, the relative errors were often 10% or less.

The direct impact of the PAH/PAH interference for the ten identified Δ2 amu PAH pairs in the LRRI data set were examined as a percentage of the molecular ion overestimate. It was necessary to roughly approximate the PAH fractionation pattern to estimate the magnitude of these impacts. For this purpose only, we assumed that the signal at the $[M\text{-}2H]^+$ ion fragment was 40% of the signal at the molecular ion $[M]^+$, based on inspection of the HR-AMS fragmentation pattern of PAH compounds. This is

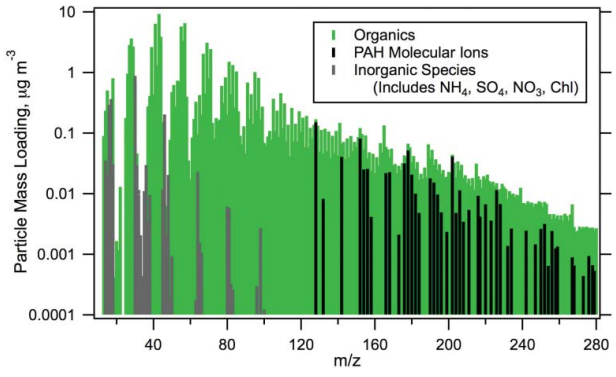

FIG. 2. HR-AMS Test04 V-mode average mass spectrum, showing the contributions of organics, lumped inorganic components (nitrate, sulfate, ammonia, and chloride), and the PAH molecular ions.

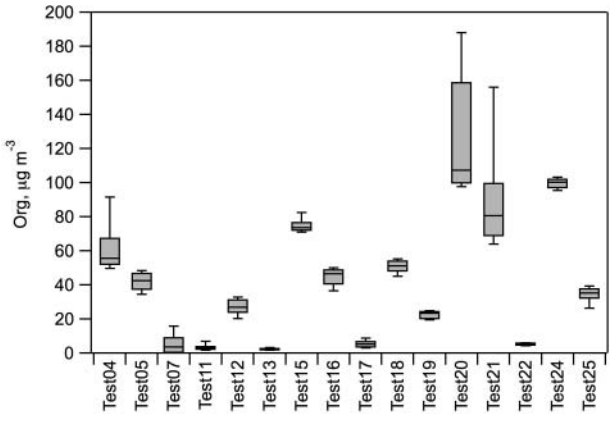

FIG. 3. HR-AMS Org concentrations for each of the LRRI experiments. Each box indicates the mean and 25th and 75th percentile, and the whiskers indicate the 10th and 90th percentile.

consistent with 25% of the total signal occurring at the molecular ions and 10% at the $[M\text{-}2H]^+$ ion. Using this assumption, we found that the magnitude of these particular PAH/PAH varied considerably. For example, because of the relatively large amount of $C_{14}H_{10}^+$ (anthracene and its isomers) molecular ion in the exhaust data, the interference to the $C_{14}H_8^+$ (paracyclene) molecular ion is also large, ~60%. However, since there is relatively little of the $C_{14}H_{12}^+$ (methyl-fluorene) molecular ion measured in the exhaust, the interference to the $C_{14}H_{10}^+$ (anthracene and its isomers) molecular ion is <10%. While these interferences are not negligible, nor are they excessive. More importantly, it will be possible to constrain them effectively once PAH standard spectra are available, since the molecular ions for the interfering compounds would be measured and the fragmentation patterns known.

4.1. PAH Contributions in Exhaust Experiments

Figure 4 shows two examples, from the Test04 (Figure 4a) and Test21 (Figure 4b) experiments, of the HR-AMS time series of Org and CO_2, alongside the summed molecular ion contributions of PAH, UnSubPAH, MPAH, OPAH, NPAH, and APAH (for the species included in this study). The CO_2 concentration (in ppm), measured by the Li-Cor 840A analyzer in tandem to the HR-AMS, is also included for Test04 to demonstrate that the temporal fluctuations are a true indication of the system dynamics and not an artifact of a single instrument (simultaneous CO_2 measurements were not available for Test21). It is apparent that each of the PAH subgroups and the total molecular ion concentrations closely follow the temporal fluctuations seen in the Org and CO_2 signal. Although only two experiments are shown, this trend was observed for all of the LRRI experiments, and holds even over two orders of magnitude change in the total Org signal. The results show clean signal above the typical HR-AMS detection limit even for the least abundant PAH molecular ion categories, NPAHs and APAHs, which have mean concentrations of ~10 and 5 ng m^{-3}, respectively, in the experiments shown in Figure 4. Figure 5 shows the PAH subgroup data expressed as a fraction of the total PAH molecular ion concentration. The relative fractions of each PAH subgroup remains approximately constant despite the temporal fluctuations in the absolute concentrations. Even more noteworthy is that when the relative fraction of any particular PAH subgroup is compared between experiments (Table S6, see the supplemental information), the variation is small, despite the mixing of different amounts of gas and diesel and the variations in engine loads as described in Table S1. Comparison of the calculated mean values for the ratios UnSubPAH/PAH, MPAH/PAH, NPAH/PAH, OPAH/PAH, and APAH/PAH across the 16 tests demonstrate that the PAH subgroup ratios do not vary significantly across temporal variations in the measured Org signal or across variations in engine operating conditions (the variance, or σ^2 of

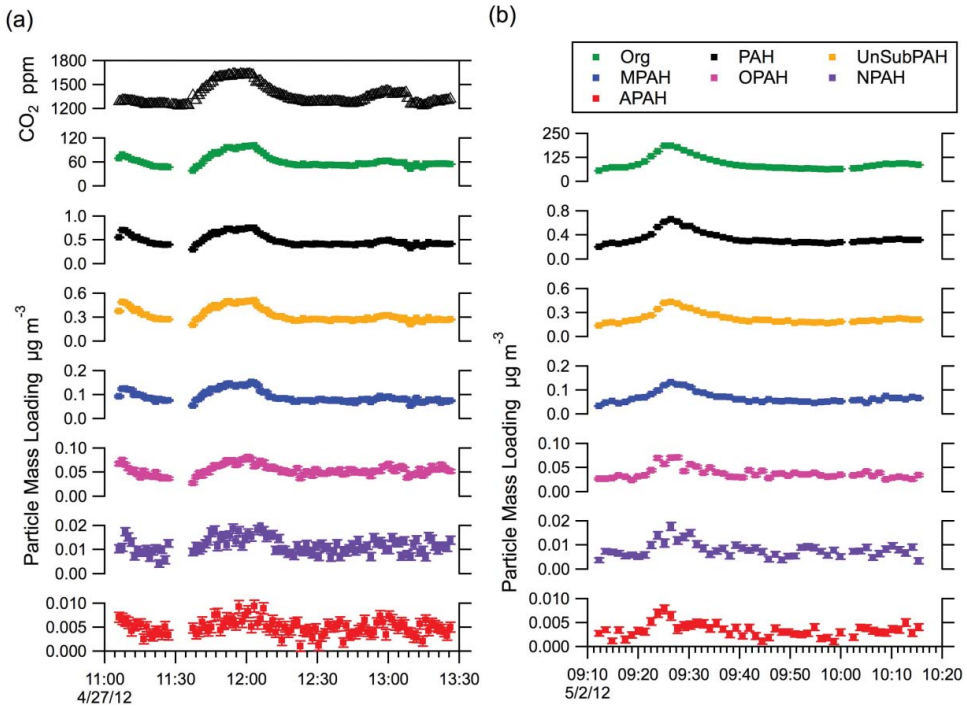

FIG. 4. Time series for (a) Test04 and (b) Test21. Shown are the gas phase CO_2 concentration (Test04 only), HR-AMS Org, and the summed total molecular ion PAH contributions and the total for each of the PAH subcategories. Error bars reflect the instrument measurement error. CO_2 data were not available for Test21.

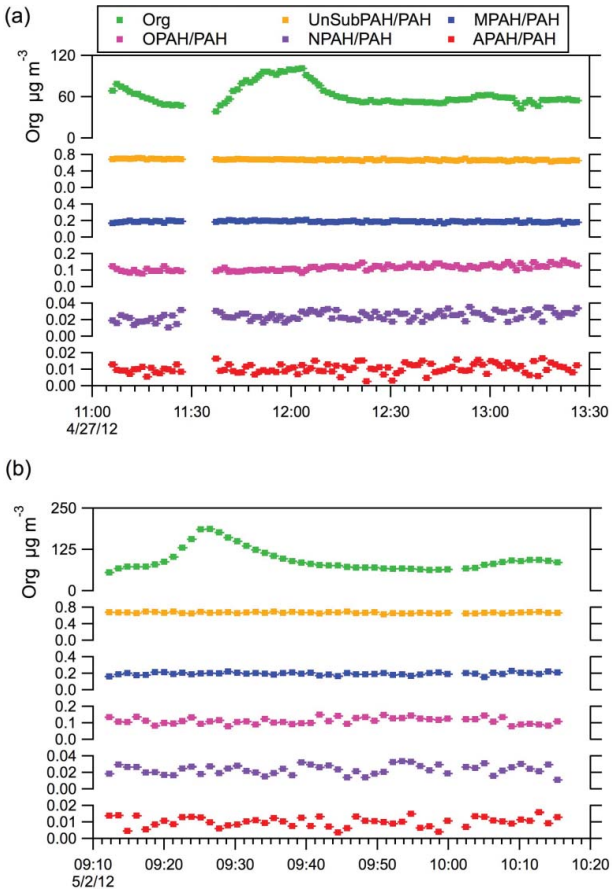

FIG. 5. Time series for the total organic signal (Org) and the total molecular ion contributions for each PAH sub-group relative to the total PAH molecular ion signal (UnSubPAH/PAH, MPAH/PAH, NPAH/PAH, OPAH/PAH, and APAH/PAH). Shown are data for (a) Test04 and (b) Test21. Error bars reflect insturment measurement error.

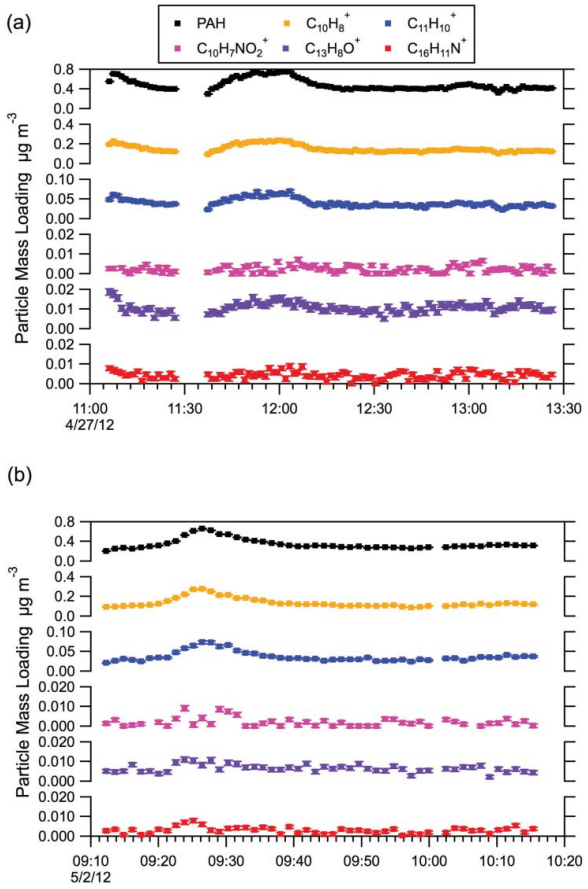

FIG. 6. Time series for the total PAH molecular ion signal (PAH) and the individual molecular ion signals for select individual PAHs: naphthalene ($C_{10}H_8^+$), methylnaphthalene ($C_{11}H_{10}^+$), nitronaphthalene ($C_{10}H_7NO_2^+$), fluorenone ($C_{13}H_8O^+$), and aminopyrene ($C_{16}H_{11}N^+$). Shown are data for (a) Test04 and (b) Test21. Error bars reflect instrument measurement error.

the aforementioned PAH subgroup ratios ranged between 2.25×10^{-6} and 1.21×10^{-4}). This suggests that changes in engine operations, or even switching from a diesel-dominated to gasoline-dominated regime, did not impact the relative formation of any subgroup of PAH compounds.

The strong correlations observed for PAH categories in Figure 5 can also be seen in individual molecular ions. Figure 6 shows the time series for five such ions – naphthalene ($C_{10}H_8^+$), methylnaphthalene ($C_{11}H_{10}^+$), nitronaphthalene ($C_{10}H_7NO_2^+$), aminopyrene ($C_{16}H_{11}N^+$), and fluorenone ($C_{13}H_8O^+$), along with the time series for the total PAH molecular ion concentration. The figures shows that the same time variations seen in the total PAH signal are also observed for individual PAH molecular ions.

4.2. Mass Composition and Concentration Across Exhaust Experiments

The ratios of PAH categories and individual ions are strongly correlated with the total PAH molecular ion concentration within each experiment, and these ratios are consistent from experiment to experiment. The ratio of total PAH molecular ion signal to the total Org signal (PAH/Org) is also very stable within individual experiments (Figure 7). However, unlike the ratios of the PAH subgroups, there was considerable variation in the PAH/Org ratio experiment-to-experiment. So while the profile of PAHs is remarkably stable across all of the LRRI tests, the amount of total PAHs relative to the total organic aerosol shows significant variability.

Based on previous work showing that PAH emissions during combustion were a function of engine operating conditions, variability in the PAH/Org ratio is not especially surprising. Indeed, the consistency in the PAH profile is probably more noteworthy. We examined several factors related to engine operation in an attempt to identify the drivers for the observed PAH/Org variability. Factors examined included engine load, the relative amounts of gasoline and diesel exhaust, and the amount of dilution used in generating the exhaust mixture. No significant trends could be observed for any of these factors. The two panels of Figure 8 compare the PAH and Org concentrations for

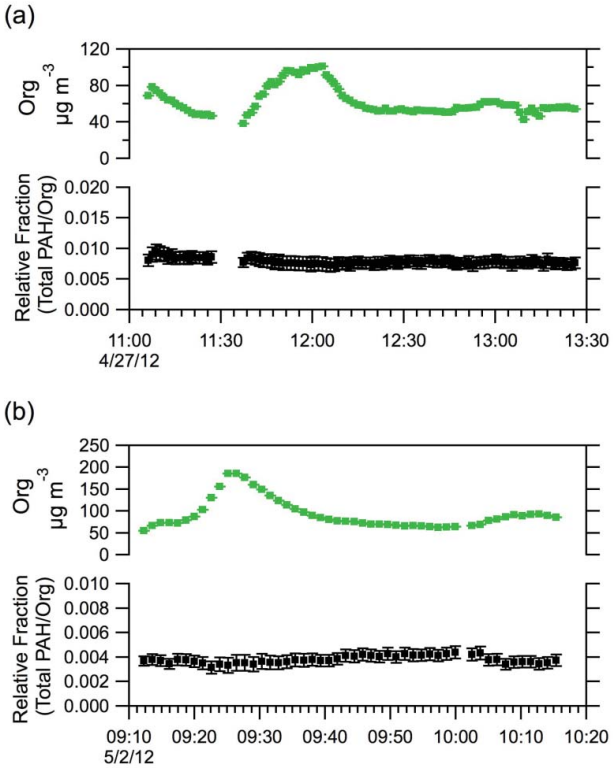

FIG. 7. Time series of the total HR-AMS organic signal (Org) and the ratio of total PAH molecular ion signals to the total organic signal (PAH/Org) for (a) Test04 and (b) Test21. Error bars reflect instrument measurement error.

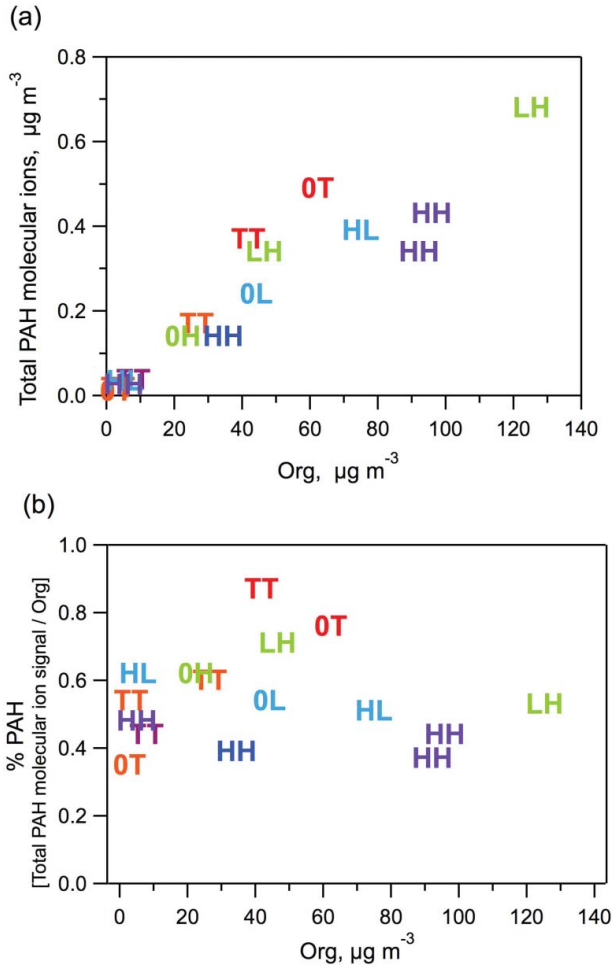

FIG. 8. Scatter plots comparing PAH signals at different engine test conditions. Plots relate (a) the total PAH molecular ion mass loading to the total measured organic mass loading (Org); and (b) the relative total PAH molecular ion mass load (% PAH) to the total measured organic mass load (Org). Indicators with the same hue designate tests performed in the same day. Symbols indicate the gasoline engine load and diesel engine load, as described in the text.

different experiments. The markers incorporate three additional factors that might be expected to influence the PAH/Org ratio. The first character in each marker represents the gasoline engine load (0 = no gasoline exhaust, L = low load, T = typical load, and H = high load) and the second character represents the diesel engine load. These conditions can also be referenced in Table S1 as the "Engine Load Type" (see the supplemental information). The symbol color groups tests conducted on the same day. Figure 8a shows that there is a fairly strong correlation between total PAH molecular ion signal and the total Org ($r^2 = 0.86$). Consequently, from Figure 8b we find that there is not a strong correlation between the relative contribution of the PAH molecular ions signal and the total Org ($r^2 = 0.31$). Moreover, we do not see any clear pattern linking the observed variability to engine operating conditions, except for possibly changes related specifically to the day of measurement – similarly colored points tend to have similar PAH/Org ratios. We have no physical interpretation for these results; the engines and lab facilities were run according to the same protocols each day. Although not shown, several other comparisons were attempted without producing informative results. More work is needed to resolve whether and how factors related to engine operations can influence the profile of PAHs and their relative abundance within vehicle exhaust.

4.3. PAH Measurement Intercomparison

PAHs adsorbed onto the particle surfaces were measured during the LRRI study using a PAS 2000CE (EcoChem Analytics, League City, TX, USA). Periods of overlap between PAS and HR-AMS PAH measurements were limited, but in a few instances it was possible to compare measurements between the two instruments. Figure 9 shows the time variability for both the HR-AMS measurements and PAS measurements; r^2 values ranged between 0.76 (in Test17) to 0.98 (in Test24). However, while there was clearly a correlation between the P-MIP derived PAH molecular ion concentration and the PAS-measured surface PAH concentration for each of these individual tests, there were inconsistencies in the ratio of the HR-AMS-measured concentration to the PAS-measured concentration between tests. In Test12 and Test17, the ratio of

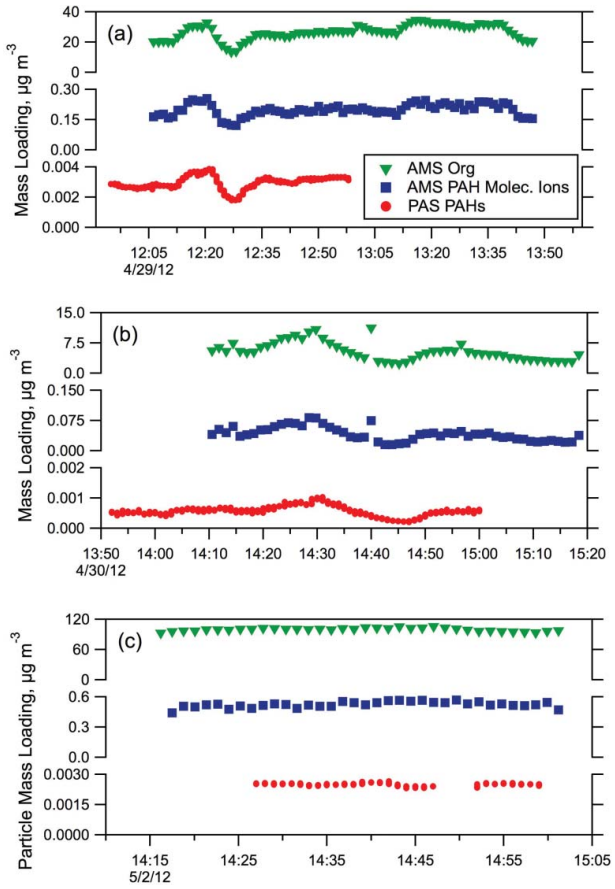

FIG. 9. Time series of HR-AMS Org, HR-AMS total PAH molecular ions, and PAS PAHs for (a) Test 12; (b) Test17; (c) Test24.

HR-AMS PAH molecular ion concentration to average surface PAH concentration was 67. During Test24, the ratio was 208.

The source of this discrepancy is not clear. It may simply be that one or both instruments' sensitivities to PAHs changed over the course of the study – neither instrument was calibrated against PAHs while at LRRI. Alternatively, the differences may instead be due to differences in their measurement approaches. The PAS specializes in measuring only the surface concentration of PAHs, and even then not all PAH species are measured (e.g., the PAS is not sensitive to naphthalene). The PAS is also more sensitive to larger PAH molecules due to their relative intensity of the signal produced by the larger PAH versus the smaller compounds. Without the ability to calibrate to precise PAH mixtures, it is difficult to definitively eliminate measurement bias based on PAH size. Performance of the PAS 2000CE has been previously documented by Marr et al. (2004, 2006).

5. CONCLUSIONS

In this study, a new methodology for the real-time characterization of speciated PAH compounds in the aerosol phase was developed that takes advantage of the measurement capabilities of the Aerodyne HR-AMS. A target list of 53 relevant PAH compounds was generated based on their previous identification in engine exhaust or their association with high carcinogenic health risk. These compounds, ranging between *m/z* 128 and *m/z* 279, included 15 UnSubPAHs, 15 OPAHs, 12 MPAHs, 7 NPAHs, and 4 APAHs. An additional 2490 near-neighbor ions were also added to facilitate accurate fitting of the target PAH ions. The P-MIP analysis was tested using a set of chamber mixed engine exhaust data collected at LRRI during April–May 2012.

To better account for the contribution of PAHs in the mixed engine exhaust, potential interferences to the PAH molecular ion signals were identified. Non-PAH interferences were found to be generally unimportant due to the high *m/z* resolution of the HR-AMS. ^{13}C isotopic interferences are well constrained by the unambiguous measurements of dominant isotope ions and known isotopic relative abundances. The potential impact of PAH/PAH interferences is small and based on available data would typically bias the results by 1% or less. The case data showed that for a few select PAH molecular ions, there was an increased occurrence of interference when two PAHs (UnSubPAH or MPAH) were separated by 2 amu. If uncorrected, the resulting bias would range between approximately 10% and 60% for this dataset, but in fact the contributions of each molecular parent could be corrected readily when PAH standard spectra are available.

Using P-MIP analysis, we have shown that it is possible to generate high-resolution time-series data of the PAH molecular ions, of summed PAH subgroups, and of individual PAH molecular ion concentrations. The total PAH molecular ion concentration was correlated with the total organic mass signal and, notably, that the relative quantities of PAHs remained constant across two orders of magnitude of variation in the total organic mass. The ability to track PAH molecular ion contributions across time highlights the advantages of this new approach. However, for P-MIP analysis to be fully useful, it must be able to robustly quantify PAH concentrations, and for that to be possible, it is crucial that extensive work be carried out to characterize the response of the HR-AMS to a broad range of PAH species. These efforts will vastly increase the value of the analysis and allow for greater progress in understanding the sources of PAHs and their behavior and effects in the atmosphere.

ACKNOWLEDGMENTS

This publication was made possible by US EPA grant #RD-83479601–0. Its contents are solely the responsibility of the grantee and do not necessarily represent the official views of the US EPA. Further, US EPA does not endorse the purchase of any commercial products or services mentioned in the publication.

SUPPLEMENTAL MATERIAL

Supplemental data for this article can be accessed on the publisher's website.

REFERENCES

Adonis, M. I., Riquelme, R. M., Gil, L., Rios, C., Rodriguez, L., and Rodriguez, E. M. (2003). PAHs and Mutagenicity of Inhalable and Respirable Diesel Particulate Matter in Santiago, Chile. *Polycycl. Aromat. Com.*, 23:495–514.

Aiken, A. C., DeCarlo, P. F., and Jimenez, J. L. (2007). Elemental Analysis of Organic Species with Electron Ionization High-Resolution Mass Spectrometry. *Anal. Chem.*, 79:8350–8358.

Alfarra, M. R. (2004). Insights Into Atmospheric Organic Aerosols using an Aerosol Mass Spectrometer, in *Department of Chemical Engineering*, UMIST, Manchester, UK.

Alkurdi, F., Karabet, F., and Dimashki, M. (2013). Characterization, Concentrations and Emission Rates of Polycyclic Aromatic Hydrocarbons in the Exhaust Emissions from in-Service Vehicles in Damascus. *Atmos. Res.*, 120:68–77.

Allan, J. D., Alfarra, M. R., Bower, K. N., Williams, P. I., Gallagher, M. W., Jimenez, J. L., McDonald, A. G., Nemitz, E., Canagaratna, M. R., Jayne, J. T., Coe, H., and Worsnop, D. R. (2003a). Quantitative Sampling using an Aerodyne Aerosol Mass Spectrometer 2. Measurements of Fine Particulate Chemical Composition in Two U.K. Cities. *J. Geophys. Res.*, 108:4091.

Allan, J. D., Bower, K. N., Coe, H., Boudries, H., Jayne, J. T., Canagaratna, M. R., Millet, D. B., Goldstein, A. H., Quinn, P. K., Weber, R. J., and Worsnop, D. R. (2004). Submicron Aerosol Composition at Trinidad Head, California, during ITCT 2K2: Its Relationship with Gas Phase Volatile Organic Carbon and Assessment of Instrument Performance. *J. Geophys. Res.*, 109:D23S24.

Allan, J. D., Jimenez, J. L., Williams, P. I., Alfarra, M. R., Bower, K. N., Jayne, J. T., Coe, H., and Worsnop, D. R. (2003b). Quantitative Sampling using an Aerodyne Aerosol Mass Spectrometer 1. Techniques of Data Interpretation and Error Analysis. *J. Geophys. Res.*, 108:4090.

Atkinson, R., and Arey, J. (1994). Atmospheric Chemistry of Gas-Phase Polycyclic Aromatic Hydrocarbons: Formation of Atmospheric Mutagens. *Environ. Health Persp.*, 102:117–126.

Bayona, J. M., Barcelo, D., and Albaiges, J. (1988). Characterization of Polar Substituted Polycyclic Aromatic-Compounds using High Resolution Gas-Chromatography Mass-Spectrometry Negative-Ion Chemical Ionization and Positive and Negative-Ion Thermospray Liquid-Chromatography Mass-Spectrometry. *Biomed. Environ. Mass Spectrom.*, 16:461–467.

Bezabeh, D. Z., Allen, T. M., McCauley, E. M., Kelly, P. B., and Jones, A. D. (1997). Negative Ion Laser Desorption Ionization Time-of-Flight Mass Spectrometry of Nitrated Polycyclic Aromatic Hydrocarbons. *J. Amer. Soc. Mass Spectrom.*, 8:630–636.

Bhatia, R., Lopipero, P., and Smith, A. H. (1998). Diesel Exhaust Exposure and Lung Cancer. *Epidemiology*, 9.

Bostrom, C. E., Gerde, P., Hanberg, A., Jernstrom, B., Johansson, C., Kyrklund, T., Rannug, A., Tornqvist, M., Victorin, K., and Westerholm, R. (2002). Cancer Risk Assessment, Indicators, and Guidelines for Polycyclic Aromatic Hydrocarbons in the Ambient Air. *Environ. Health Persp.*, 110:451–488.

Bruns, E. A., El Haddad, I., Keller, A., Klein, F., Kumar, N. K., Pieber, S. M., Corbin, J. C., Slowik, J. G., Brune, W. H., Baltensperger, U., and Prevot, A. S. H. (2015a). Inter-Comparison of Laboratory Smog Chamber and Flow Reactor Systems on Organic Aerosol Yield and Composition. *Atmos. Meas. Tech. Discuss.*, 8:2315–2332.

Bruns, E. A., Krapf, M., Orasche, J., Huang, Y., Zimmermann, R., Drinovec, L., Mocnik, G., El-Haddad, I., Slowik, J. G., Dommen, J., Baltensperger, U., and Prévôt, A. S. H. (2015b). Characterization of Primary and Secondary Wood Combustion Products Generated Under Different Burner Loads. *Atmos. Chem. Phys.* 15:2825–2841.

CAAA (1990). Clean Air Act Amendments of 1990. Available at http://epa.gov/oar/caa/caaa_overview.html. Accessed 26 January 26 2015.

Canagaratna, M. R., Jayne, J. T., Ghertner, D. A., Herndon, S., Shi, Q., Jimenez, J. L., Silva, P. J., Williams, P., Lanni, T., Drewnick, F., Demerjian, K. L., Kolb, C. E., and Worsnop, D. R. (2004). Chase Studies of Particulate Emissions from in-use New York City Vehicles. *Aerosol Sci. Technol.*, 38:555–573.

Canagaratna, M. R., Jayne, J. T., Jimenez, J. L., Allan, J. D., Alfarra, M. R., Zhang, Q., Onasch, T. B., Drewnick, F., Coe, H., Middlebrook, A., Delia, A., Williams, L. R., Trimborn, A. M., Northway, M. J., DeCarlo, P. F., Kolb, C. E., Davidovits, P., and Worsnop, D. R. (2007). Chemical and Microphysical Characterization of Ambient Aerosols with the Aerodyne Aerosol Mass Spectrometer. *Mass Spectrom. Rev.*, 26:185–222.

Canagaratna, M. R., Jimenez, J. L., Kroll, J. H., Chen, Q., Kessler, S. H., Massoli, P., Hildebrandt Ruiz, L., Fortner, E., Williams, L. R., Wilson, K. R., Surratt, J. D., Donahue, N. M., Jayne, J. T., and Worsnop, D. R. (2015). Elemental Ratio Measurements of Organic Compounds using Aerosol Mass Spectrometry: Characterization, Improved Calibration, and Implications. *Atmos. Chem. Phys.* 15:253–272.

Chirico, R., DeCarlo, P. F., Heringa, M. F., Tritscher, T., Richter, R., Prevot, A. S. H., Dommen, J., Weingartner, E., Wehrle, G., Gysel, M., Laborde, M., and Baltensperger, U. (2010). Impact of Aftertreatment Devices on Primary Emissions and Secondary Organic Aerosol Formation Potential from in-Use Diesel Vehicles: Results from Smog Chamber Experiments. *Atmos. Chem. Phys.*, 10:11545–11563.

Choudhury, D. R. (1982). Characterization of Polycyclic Ketones and Quinones in Diesel Emission Particulates by Gas-Chromatography Mass-Spectrometry. *Environ. Sci. Technol.*, 16:102–106.

Corbin, J. C., Othman, A., Haskins, J. D., Allan, J. D., Sierau, B., Worsnop, D. R., Lohmann, U., and Mensah, A. A. (2015). Peak Fitting and Integration Uncertainties for the Aerodyne Aerosol Mass Spectrometer. *Atmos. Meas. Tech. Discuss.*, 8:3471–3523.

Dallmann, T. R., Onasch, T. B., Kirchstetter, T. W., Worton, D. R., Fortner, E. C., Herndon, S. C., Wood, E. C., Franklin, J. P., Worsnop, D. R., Goldstein, A. H., and Harley, R. A. (2014). Characterization of Particulate Matter Emissions from on-Road Gasoline and Diesel Vehicles using a Soot Particle Aerosol Mass Spectrometer. *Atmos. Chem. Phys.*, 14: 7585–7599.

DeCarlo, P. F., Kimmel, J. R., Trimborn, A., Northway, M. J., Jayne, J. T., Aiken, A. C., Gonin, M., Fuhrer, K., Horvath, T., Docherty, K. S., Worsnop, D. R., and Jimenez, J. L. (2006). Field-Deployable, High-Resolution, Time-of-Flight Aerosol Mass Spectrometer. *Anal. Chem.*, 78:8281–8289.

Delhomme, O., Herckes, P., and Millet, M. (2007). Determination of Nitro-Polycyclic Aromatic Hydrocarbons in Atmospheric Aerosols using HPLC Fluorescence with a Post-Column Derivatisation Technique. *Anal. Bioanal. Chem.*, 389:1953–1959.

Džepina, K., Arey, J., Marr, L. C., Worsnop, D. R., Salcedo, D., Zhang, Q., Onasch, T. B., Molina, L. T., Molina, M. J., and Jimenez, J. L. (2007). Detection of Particle-Phase Polycyclic Aromatic Hydrocarbons in Mexico City using an Aerosol Mass Spectrometer. *Int. J. Mass Spectrom.*, 263:152–170.

Eriksson, A. C., Nordin, E. Z., Nystrom, R., Pettersson, E., Swietlicki, E., Bergvall, C., Westerholm, R., Boman, C., and Pagels, J. H. (2014). Particulate PAH Emissions from Residential Biomass Combustion: Time-Resolved Analysis with Aerosol Mass Spectrometry. *Environ. Sci. Technol.*, 48:7143–7150.

Fraser, M. P., Cass, G. R., and Simoneit, B. R. T. (1998). Gas-Phase and Particle-Phase Organic Compounds Emitted from Motor Vehicle Traffic in a Los Angeles Roadway Tunnel. *Environ. Sci. Technol.*, 32:2051–2060.

Frenich, A. G., Ocana, R. M., and Vidal, J. L. M. (2010). Determination of Polycyclic Aromatic Hydrocarbons in Airborne Particulate Matter by Gas

Chromatography-Triple Quadrupole Tandem Mass Spectrometry. *J. Aoac. Int.*, 93:284–294.

Fujita, E. M., Zielinska, B., Campbell, D. E., Arnott, W. P., Sagebiel, J. C., Mazzoleni, L., Chow, J. C., Gabele, P. A., Crews, W., Snow, R., Clark, N. N., Wayne, W. S., and Lawson, D. R. (2007). Variations in Speciated Emissions from Spark-Ignition and Compression-Ignition Motor Vehicles in California's South Coast Air Basin. *J. Air Waste Manag. Assoc.*, 57:705–720.

Gross, D. S., Galli, M. E., Silva, P. J., Wood, S. H., Liu, D.-Y., and Prather, K. A. (2000). Single Particle Characterization of Automobile and Diesel Truck Emissions in the Caldecott Tunnel. *Aerosol Sci. Technol.*, 32:152–163.

Harrison, R. M., Smith, D. J. T., and Luhana, L. (1996). Source Apportionment of Atmospheric Polycyclic Aromatic Hydrocarbons Collected from an Urban Location in Birmingham, UK. *Environ. Sci. Technol.*, 30: 825–832.

Hattori, T., Tang, N., Tamura, K., Hokoda, A., Yang, X., Igarashi, K., Ohno, M., Okada, Y., Kameda, T., Toriba, A., and Hayakawa, K. (2007). Particulate Polycyclic Aromatic Hydrocarbons and Their Nitrated Derivatives in Three Cities in Liaoning Province, China. *Environ. Forensic.*, 8:165–172.

He, L. Y., Hu, M., Huang, X. F., Zhang, Y. H., Yu, B. D., and Liu, D. Q. (2006). Chemical Characterization of Fine Particles from on-Road Vehicles in the Wutong Tunnel in Shenzhen, China. *Chemosphere*, 62:1565–1573.

Huang, L., Bohac, S. V., Chernyak, S. M., and Batterman, S. A. (2013). Composition and Integrity of PAHs, nitro-PAHs, Hopanes, and Steranes in Diesel Exhaust Particulate Matter. *Water Air Soil Pollut.*, 224.

Internal Agency for Research (1989). *IARC International Agency for Research on Cancer Monographs on the Evaluation of Carcinogenic Risks to Humans Vol. 46. Diesel and Gasoline Engine Exhaust and Some Nitroarenes.*

International Agency for Research (2013). *IARC International Agency for Research on Cancer Monographs on the Evaluation of Carcinogenic Risks to Humans Vol. 105. Diesel and Gasoline Engine Exhaust and Some Nitroarenes*.

Jimenez, J. L., Jayne, J. T., Shi, Q., Kolb, C. E., Worsnop, D. R., Yourshaw, I., Seinfeld, J. H., Flagan, R. C., Zhang, X. F., Smith, K. A., Morris, J. W., and Davidovits, P. (2003). Ambient Aerosol Sampling using the Aerodyne Aerosol Mass Spectrometer. *J. Geophys. Res.-Atmos.*, 108.

Kuwata, M., Zorn, S. R., and Martin, S. T. (2012). Using Elemental Ratios to Predict the Density of Organic Material Composed of Carbon, Hydrogen, and Oxygen. *Environ. Sci. Technol.*, 46:787–794.

Layshock, J. A., Wilson, G., and Anderson, K. A. (2010). Ketone and Quinone-Substituted Polycyclic Aromatic Hydrocarbons in Mussel Tissue, Sediment, Urban Dust, and Diesel Particulate Matrices. *Environ. Toxicol. Chem.*, 29:2450–2460.

Lee, M. L., Novotny, M. V., and Bartle, K. D. (1981). *Analytical Chemistry of Polycyclic Aromatic Compounds*. Academic Press, New York.

Liu, L.-b., Liu, Y., Lin, J.-m., Tang, N., Hayakawa, K., and Maeda, T. (2007). Development of Analytical Methods for Polycyclic Aromatic Hydrocarbons (PAHs) in Airborne Particulates: A Review. *J. Environ. Sci.-China*, 19:1–11.

Marr, L. C., Dzepina, K., Jimenez, J. L., Reisen, F., Bethel, H. L., Arey, J., Gaffney, J. S., Marley, N. A., Molina, L. T., and Molina, M. J. (2006). Sources and Transformations of Particle-Bound Polycyclic Aromatic Hydrocarbons in Mexico City. *Atmos. Chem. Phys.*, 6:1733–1745.

Marr, L. C., Grogan, L. A., Wohrnschimmel, H., Molina, L. T., Molina, M. J., Smith, T. J., and Garshick, E. (2004). Vehicle Traffic as a Source of Particulate Polycyclic Aromatic Hydrocarbon Exposure in the Mexico City Metropolitan Area. *Environ. Sci. Technol.*, 38:2584–2592.

Massoli, P., Fortner, E. C., Canagaratna, M. R., Williams, L. R., Zhang, Q., Sun, Y., Schwab, J. J., Trimborn, A., Onasch, T. B., Demerjian, K. L., Kolb, C. E., Worsnop, D. R., and Jayne, J. T. (2012). Pollution Gradients and Chemical Characterization of Particulate Matter from Vehicular Traffic Near Major Roadways: Results from the 2009 Queens College Air Quality Study in NYC. *Aerosol Sci. Technol.*, 46:1201–1218.

Matthew, B. M., Middlebrook, A. M., and Onasch, T. B. (2008). Collection Efficiencies in an Aerodyne Aerosol Mass Spectrometer as a Function of Particle Phase for Laboratory Generated Aerosols. *Aerosol Sci. Technol.*, 42:884–898.

McDonald, J. (2005). Diesel and Gasoline Engine Emissions: Characterization of Atmosphere Composition and Health Responses to Inhaled Emissions. Available at http://www1.eere.energy.gov/vehiclesandfuels/pdfs/deer_2005/session2/2005_deer_mcdonald.pdf. Accessed 20 March 2014.

McDonald, J., Harrod, K., Seagrave, J., Seilkop, S., and Mauderly, J. (2003). The Effect of Changes in Diesel Exhaust Composition and After-Treatment Technology on Lung Inflammation and Resistance to Viral Infection. Available at http://www1.eere.energy.gov/vehiclesandfuels/pdfs/deer_2003/session9/2003_deer_mcdonald.pdf. Accessed 20 March 2014.

McDonald, J. D., Barr, E. B., and White, R. K. (2004a). Design, Characterization, and Evaluation of a Small-Scale Diesel Exhaust Exposure System. *Aerosol Sci. Technol.*, 38:62–78.

McDonald, J. D., Barr, E. B., White, R. K., Chow, J. C., Schauer, J. J., Zielinska, B., and Grosjean, E. (2004b). Generation and Characterization of Four Dilutions of Diesel Engine Exhaust for a Subchronic Inhalation Study. *Environ. Sci. Technol.*, 38:2513–2522.

McDonald, J. D., Campen, M. J., Harrod, K. S., Seagrave, J., Seilkop, S. K., and Mauderly, J. L. (2011). Engine-Operating Load Influences Diesel Exhaust Composition and Cardiopulmonary and Immune Responses. *Environ. Health Persp.*, 119:1136–1141.

Mi, H. H., Lee, W. J., Tsai, P. J., and Chen, C. B. (2001). A Comparison on the Emission of Polycyclic Aromatic Hydrocarbons and Their Corresponding Carcinogenic Potencies from a Vehicle Engine using Leaded and Lead-Free Gasoline. *Environ. Health Persp.*, 109:1285–1290.

Mohr, C., Huffman, J. A., Cubison, M. J., Aiken, A. C., Docherty, K. S., Kimmel, J. R., Ulbrich, I. M., Hannigan, M., and Jimenez, J. L. (2009). Characterization of Primary Organic Aerosol Emissions from Meat Cooking, Trash Burning, and Motor Vehicles with High-Resolution Aerosol Mass spectrometry and comparison with ambient and chamber observations. *Environ. Sci. Technol.*, 43:2443–2449.

Mueller, L., Jakobi, G., Orasche, J., Karg, E., Sklorz, M., Abbaszade, G., Weggler, B., Jing, L. P., Schnelle-Kreis, J., and Zimmermann, R. (2015). Online Determination of Polycyclic Aromatic Hydrocarbon Formation from a Flame Soot Generator. *Anal. Bioanal. Chem.*, 407:5911–5922.

Nelson, P. F., Tibbett, A. R., and Day, S. J. (2008). Effects of Vehicle Type and Fuel Quality on Real World Toxic Emissions from Diesel Vehicles. *Atmos. Environ.*, 42:5291–5303.

NIST mass spec data center. (2014). Stein, S.E. (director), "Mass Spectra" in NIST Chemistry WebBook, NIST standard reference database number 69, Eds. P.J. Linstrom and W.G. Mallard, National Institute of Standards and Technology, Gaithersburg MD, 20899. http://webbook.nist.gov. Accesed 12 November 2014.

Pandey, S. K., Kim, K. H., and Brown, R. J. C. (2011). A Review of Techniques for the Determination of Polycyclic Aromatic Hydrocarbons in Air. *Trac-Trends Anal. Chem.*, 30:1716–1739.

Patiny, L., and Borel, A. (2013). ChemCalc: A Building Block for Tomorrow's Chemical Infrastructure. *J. Chem. Informat. Mod.*, 53:1223–1228.

Polidori, A., Hu, S., Biswas, S., Delfino, R. J., and Sioutas, C. (2008). Real-Time Characterization of Particle-Bound Polycyclic Aromatic Hydrocarbons in Ambient Aerosols and from Motor-Vehicle Exhaust. *Atmos. Chem. Phys.*, 8:1277–1291.

Pope, C. A., Burnett, R. T., Thun, M. J., Calle, E. E., Krewski, D., Ito, K., and Thurston, G. D. (2002). Lung Cancer, Cardiopulmonary Mortality, and Long-Term Exposure to Fine Particulate Air Pollution. *Jama.-J. Am. Med. Assoc.*, 287:1132–1141.

Poster, D. L., Benner, B. A., Schantz, M. M., Sander, L. C., Wise, S. A., and Vangel, M. G. (2003). Determination of Methyl-Substituted Polycyclic Aromatic Hydrocarbons in Diesel Particulate-Related Standard Reference Materials. *Polycycl. Aromat. Com.*, 23:113–139.

Pratt, K. A., and Prather, K. A. (2011). Mass Spectrometry of Atmospheric Aerosols—Recent Developments and Applications. Part I: Off-Line Mass Spectrometry Techniques. *Mass Spectrom. Rev.*, 31:1–16.

Rajput, N., and Lakhani, A. (2009). PAHs and Their Carcinogenic Potencies in Diesel Fuel and Diesel Generator Exhaust. *Human Ecol. Risk Assess.*, 15:201–213.

Ramdahl, T. (1983). Polycyclic Aromatic Ketones in Environmental Samples. *Environ. Sci. Technol.*, 17:666–670.

Rappaport, S. M., Wang, Y. Y., Wei, E. T., Sawyer, R., Watkins, B. E., and Rapoport, H. (1980). Isolation and Identification of a Direct-Acting Mutagen in Diesel-Exhaust Particles. *Environ. Sci. Technol.*, 14:1505–1509.

Ravindra, K., Sokhi, R., and Van Grieken, R. (2008). Atmospheric Polycyclic Aromatic Hydrocarbons: Source Attribution, Emission Factors and Regulation. *Atmos. Environ.*, 42:2895–2921.

Ringuet, J., Albinet, A., Leoz-Garziandia, E., Budzinski, H., and Villenave, E. (2012). Reactivity of Polycyclic Aromatic Compounds (PAHs, NPAHs and OPAHs) Adsorbed on Natural Aerosol Particles Exposed to Atmospheric Oxidants. *Atmos. Environ.*, 61:15–22.

Rogge, W. F., Hildemann, L. M., Mazurek, M. A., Cass, G. R., and Simoneit, B. R. T. (1993). Sources of Fine Organic Aerosol. 2. Noncatalyst and Catalyst-Equipped Automobiles and Heavy-Duty Diesel Trucks. *Environ. Sci. Technol.*, 27:636–651.

Sasaki, J., Aschmann, S. M., Kwok, E. S. C., Atkinson, R., and Arey, J. (1997). Products of the Gas-Phase OH and NO3 Radical-Initiated Reactions of Naphthalene. *Environ. Sci. Technol.*, 31:3173–3179.

Schauer, J. J., Kleeman, M. J., Cass, G. R., and Simoneit, B. R. T. (1999). Measurement of Emissions from Air Pollution Sources. 2. C-1 Through C-30 Organic Compounds from Medium Duty Diesel Trucks. *Environ. Sci. Technol.*, 33:1578–1587.

Schauer, J. J., Kleeman, M. J., Cass, G. R., and Simoneit, B. R. T. (2002). Measurement of Emissions from Air Pollution Sources. 5. C-1-C-32 Organic Compounds from Gasoline-Powered Motor Vehicles. *Environ. Sci. Technol.*, 36:1169–1180.

Schuetzle, D., Lee, F. S. C., Prater, T. J., and Tejada, S. B. (1981). The Identification of Polynuclear Aromatic Hydrocarbon (PAH) Derivatives in Mutagenic Fractions of Diesel Particulate Extracts. *Int. J. Environ. Anal. Chem.*, 9:93–144.

Shah, S. D., Cocker, D. R., Miller, J. W., and Norbeck, J. M. (2004). Emission Rates of Particulate Matter and Elemental and Organic Carbon from in-Use Diesel Engines. *Environ. Sci. Technol.*, 38:2544–2550.

Sienra, M. D. (2006). Oxygenated Polycyclic Aromatic Hydrocarbons in Urban Air Particulate Matter. *Atmos. Environ.*, 40:2374–2384.

Sienra, M. D., and Rosazza, N. G. (2006). Occurrence of Nitro-Polycyclic Aromatic Hydrocarbons in Urban Particulate Matter PM10. *Atmos. Res.*, 81:265–276.

Silva, P. J., and Prather, K. A. (2000). Interpretation of Mass Spectra from Organic Compounds in Aerosol Time-of-Flight Mass Spectrometry. *Anal. Chem.*, 72:3553–3562.

Slowik, J. G., Stainken, K., Davidovits, P., Williams, L. R., Jayne, J. T., Kolb, C. E., Worsnop, D. R., Rudich, Y., DeCarlo, P. F., and Jimenez, J. L. (2004). Particle Morphology and Density Characterization by Combined Mobility and Aerodynamic Diameter Measurements. Part 2: Application to Combustion-Generated Soot Aerosols as a Function of Fuel Equivalence Ratio. *Aerosol Sci. Technol.*, 38:1206–1222.

Sodeman, D. A., Toner, S. M., and Prather, K. A. (2005). Determination of Single Particle Mass Spectral Signatures from Light-Duty Vehicle Emissions. *Environ. Sci. Technol.*, 39:4569–4580.

Strandell, M., Zakrisson, S., Alsberg, T., Westerholm, R., Winquist, L., and Rannug, U. (1994). Chemical-Analysis and Biological Testing of a Polar Fraction of Ambient Air, Diesel-Engine, and Gasoline-Engine Particulate Extracts. *Environ. Health Persp.*, 102:85–92.

Sueper, D. (2010). ToF-AMS Analysis Software. Available at http://cires.colorado.edu/jimenez-group/ToFAMSResources/ToFSoftware/index.html. Accessed 3 October 2014.

Sueper, D. (2014). HR Error Estimates. Available at http://cires1.colorado.edu/jimenez-group/ToFAMSResources/ToFSoftware/PikaNotes/HRErrorEstimates.pdf. Accessed 28 August 2015.

Timko, M. T., Albo, S. E., Onasch, T. B., Fortner, E. C., Yu, Z., Miake-Lye, R. C., Canagaratna, M. R., Ng, N. L., and Worsnop, D. R. (2014). Composition and Sources of the Organic Particle Emissions from Aircraft Engines. *Aerosol Sci. Technol.*, 48:61–73.

Timko, M. T., Yu, Z., Kroll, J., Jayne, J. T., Worsnop, D. R., Miake-Lye, R. C., Onasch, T. B., Liscinsky, D., Kirchstetter, T. W., Destaillats, H., Holder, A. L., Smith, J. D., and Wilson, K. R. (2009). Sampling Artifacts from Conductive Silicone Tubing. *Aerosol Sci. Technol.*, 43:855–865.

Tobias, H. J., Beving, D. E., Ziemann, P. J., Sakurai, H., Zuk, M., McMurry, P. H., Zarling, D., Waytulonis, R., and Kittelson, D. B. (2001). Chemical Analysis of Diesel Engine Nanoparticles using a Nano-DMA/Thermal Desorption Particle Beam Mass Spectrometer. *Environ. Sci. Technol.*, 35:2233–2243.

Ulbrich, I. M., Canagaratna, M. R., Zhang, Q., Worsnop, D. R., and Jimenez, J. L. (2009). Interpretation of Organic Components from Positive Matrix Factorization of Aerosol Mass Spectrometric Data. *Atmos. Chem. Phys.*, 9:2891–2918.

Ulbrich, I. M., Lechner, M., and Jimenez, J. L. (2007). AMS Spectral Database. Available at http://cires.colorado.edu/jimenez-group/AMSsd./ Accessed 10 August 2015.

US EPA (1992). Suspect Chemical Sourcebook, in *EPA Human Health Assessment Group Substances*, Roytech, Bethesda, MD.

Vincenti, M., Minero, C., Pelizzetti, E., Fontana, M., and DeMaria, R. (1996). Sub-Parts-Per-Billion Determination of Nitro-Substituted Polynuclear Aromatic Hydrocarbons in Airborne Particulate Matter and Soil by Electron Capture-Tandem Mass Spectrometry. *J. Amer. Soc. Mass Spectrom.*, 7:1255–1265.

Wang, W. G., Lyons, D. W., Clark, N. N., Gautam, M., and Norton, P. M. (2000). Emissions from Nine Heavy Trucks Fueled by Diesel and Biodiesel Blend Without Engine Modification. *Environ. Sci. Technol.*, 34:933–939.

Zielinska, B., Sagebiel, J., McDonald, J. D., Whitney, K., and Lawson, D. R. (2004). Emission Rates and Comparative Chemical Composition from Selected in-Use Diesel and Gasoline-Fueled Vehicles. *J. Air Waste Manag. Assoc.*, 54:1138–1150.

Zielinska, B., and Samy, S. (2006). Analysis of Nitrated Polycyclic Aromatic Hydrocarbons. *Anal. Bioanal. Chem.*, 386:883–890.